TotalControl

Advanced integrated supervisory and wind turbine control for optimal operation of large Wind Power Plants

Electrical/Mechanical/Control Interactions in Large Wind Power Plants.
Deliverable no. D4.6

Delivery date: 31.05.2022
Lead beneficiary: SINTEF Energy Research
Dissemination level: Public

Author(s) information (alphabetical):		
Name	Organisation	Email
Kölle, Konstanze	SINTEF Energy Research	konstanze.koelle@sintef.no
Merz, Karl	SINTEF Energy Research	karl.merz@sintef.no
Nwobu, John	ORE Catapult	john.nwobu@ore.catapult.org.uk

Acknowledgements/Contributions:		
Name	Name	Name

Document information

Version	Date	Description			
			Prepared by	Reviewed by	Approved by
1.0	19.05.2022	Original	K. Merz, J. Nwobu, K. Kölle		

Definitions

Contents

ATTACHMENTS

PROJECT
TotalControl

REPORT NUMBER
D4.6

VERSION
1.0

3 of 47

1 Executive summary

Modern (offshore) wind power plants have large installed capacities which can have a significant effect on the power system they are connected to. Electrical-mechanical-control interactions between wind turbines and the grid can pose a risk on the stable and reliable operation of the power system. This report is divided into two parts studying different aspects of grid integration.

The first part studies the provision of reactive power by wind power plants at the example of the TotalControl Reference Wind Power Plant (TC-RWP). Benchmark results from the H2020 FarmConners project are utilised for the active power gain to define the set-up of the present simulation study combining reactive control and wake steering. The results highlight the importance of reactive power control when farm flow control is integrated in existing wind farm control systems. Guidance for the development of such integrated wind farm control is provided to ensure that the wind turbines will still be operated within their design limits.

The second part investigates dynamic interactions of a wind power plant with a thermal power plant and a hydroelectric power plant. These power plants are assumed connected at a common bus to both a strong grid and an isolated load. The TC-RWP is again applied as example. It is found that the dynamic interactions between the plants are limited when the grid is strong. In the case of a weak or isolated grid, the dynamics of the different generating units are coupled. In particular, hydraulic modes associated with the hydroelectric plant restrict its ability to provide frequency support and could influence the wind turbine pitch actuator duty. The wind turbines' tower modes are felt by the thermal plant, and this could be problematic in the event that the turbines' vibrations were synchronized.
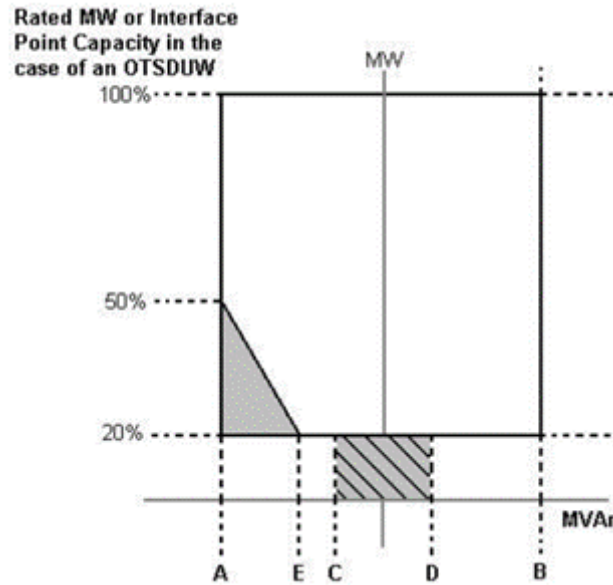
PROJECT
TotalControl

REPORT NUMBER
D4.6

VERSION
1.0

4 of 47

Figure 1: Examples of P, Q operation conditions as in the grid code (National Grid ESO (2019), The Grid Code).

2   Reactive power system studies

Wind Farm Control (WFC) is an umbrella term that is used in different contexts and applications (Eguinoa *et al.* 2021). It is at times referred to as Wind Farm Grid Control (WF-GC) as suggested in the Total Control Deliverable 4.7 (Hille *et al.* 2020) where this aims to control features that ensure that wind turbines comply with local grid codes and grid integration requirements. In other cases, this can be used when describing Wind Farm Flow Control (WF-FC) which aims at maximising power extraction and alleviating loads on wind turbines. In general, WFC is the operation of a whole wind farm in a coordinated way, for example, by using models.

Optimal control of reactive power in wind farms is important in ensuring losses of power are minimised in the wind farm. This part focuses on reactive power system studies of using the Total Control Reference Wind Power Plant (TC-RWP) developed as part of the work and activities in the project (Andersen *et al.* 2018). This takes into consideration the use of available data sets and results from the high fidelity wake steering simulations performed as part of the project (Andersen *et al.* 2020). The power system for the wake steering models has been developed in a high-fidelity power system modelling software (PSCAD) and reactive power studies are undertaken to understand the performance of the wind turbines under waked conditions.

2.1   Reactive power and voltage support

Reactive power dispatch between the wind turbines in a wind farm is important so that the total electrical losses in the wind farm electrical infrastructure are minimized (TotalControl D2.3). Historically, electricity system operators have accessed reactive power and voltage support for their power networks by setting adequate connection requirements for network users in the relevant grid network codes. During normal operation, the system operator (SO) usually has the right to control the power factor or the reactive power at the Grid Connection i.e., the point of connection (PoC). These requirements by the SO have to be met by the wind farm operator. With the advancement of new techniques in WFC such as wake steering, the WFC still needs to ensure that the control principles of wind farms comply to the grid code and connection agreements.

2.1.1 Grid code compliance (GCC)

Grid or Network Codes are regulations that provide the framework and rules for operating electricity transmission and distribution networks. Among other conditions, they set acceptable operational ranges for a number of electrical parameters at the point of common coupling between a wind farm and the network. In this way, the grid codes impose control response capability requirements on any user seeking connection rights. The state of the art of grid codes is documented in various international standards, national rules, governmental orders. Fulfilling and complying to those requirements is what is referred to as Grid Code Compliance (GCC). In some cases, the requirements are applicable to all generators within a given power/voltage range independently of the technology of choice. In other cases, the requirements are specific for a given generation technology, e.g.. intermittent sources like onshore and offshore wind farms. Generators applying for connection agreements have to ensure grid code compliance for their assets, which generally includes some form of active power (P) and reactive power (Q) response control in normal operation. In the UK for instance, the Grid Code (National Grid ESO (2019), The Grid Code) and CUSC – Connection and Use of System Charges (National Grid ESO, 2019, Connection and Use of System Code) set up these conditions in the form of active power and frequency ramps, acceptable (P,Q) operational envelops, or others. Figure 1 presents some examples. At EU level, equivalent requirements are set up in the Requirements for Generators (ENTSO-E, 2016) and the additional documents related to its implementation by Member States.

2.1.2 Reactive power GCC features

Requirements for GCC set out in the grid codes are mostly functionalities implemented in the wind turbine or the WF-GC intended to maintain the performance of electrical characteristics. These functionalities are called GCC features. A crucial aspect in the TotalControl project is understanding the limitations of controllability of these GCC features in order to comply with the grid code when implementing WFC.

A list of GCC features descriptions for various grid codes are collected in the grid code listing (DNV, 2022). As not all of those GCC features are relevant within this report, only those which deem to be relevant to reactive power support are listed below. These are grouped according to the types of features as shown below in Table I.

- R – Rating and Design Related GCC Features

- D – Dynamic GCC Features (Reactive Power Control etc.)

2.1.3 Reactive power services – UK perspective

Historically, reactive power services have been provided by big synchronous generators operating in conventional power plants. Electricity system operators procure these services from generators that are available when required from the control room. These services are procured to make sure voltage levels on the system remain within a given range, above or below nominal voltage levels. This is maintained by either instructing generators or other asset owners to either absorb or generate reactive power either within or in excess of the minimum requirements in the contract (as per the grid code).

In the UK, there are currently two services procured listed below Obligatory reactive power service (ORPS): This provides a varying reactive power output, and any given generator may be requested to produce or absorb reactive power to maintain the systems' voltages at the point of connection (PoC). In such situations, generators must be capable of supplying their rated power output (MW) at any point between the limits 0.85 power factor lagging and 0.95 power factor leading. Generally, all power stations connected to the transmission network with a generation capacity of over 50 MW are required to have the capability to provide this service, as set out in the Grid Code.

PROJECT
TotalControl

REPORT NUMBER
D4.6

VERSION
1.0

6 of 47

	Feature	Description
R1	U/f/P/t-figure	A voltage-frequency-power-time figure relating to the WT design. Corresponding figures (or corresponding tables or pure descriptions) are specifying the operating area for simultaneous values of voltage, frequency, output power and time.
R5	Reactive power rating for both WT and WF design	The steady-state reactive power capability shall be specified in a PQ-chart. The PQ-chart shall be valid for the full active power operating area. The reactive power capability versus the grid operation voltage in the PoC including the effects of voltage control shall be specified in a single UQ-chart.
D9	Power factor control mode	Reactive power of each WT is coordinated by the WF-GC in order to achieve the desired power factor as requested via remote control by the SO to be set at the wind farm's PoC.
D10	reactive power control mode	Reactive power of each WT is coordinated by the WF-GC in order to achieve the desired reactive power value as requested via remote control by the SO to be set at the wind farm's PoC.
D11	Voltage control mode	Reactive power of each WT is coordinated by the WF-GC in order to achieve the desired voltage value as requested via remote control by the SO to be set at the wind farm's PoC.

Table I: List of reactive power GCC features descriptions for various grid codes (DNV, 2022).

Technology affected	Key blocker	Key enabler	Preferred solution
Batteries/converter connected storage	High opportunity costs in valuable/high demand periods	Need to allow plant to participate when service is most valuable	**Short term market**
Variable converter connected technologies (e.g. wind)	Low availability certainty	Need to allow plant to participate at point where availability becomes more visible/certain	**Short term market**
Traditional thermal providers	High and uncertain fuel cost + uncertain requirement (difficult to hedge)	Need to allow plant to participate when costs are known and when requirements are highest	**Short term market**
All capacity	Additional Capex and Opex associated with higher MVA rating of equipment (if relevant)	If there is a low incremental cost, but long term commitment is inappropriate need to allow some short-term revenue to encourage deployment	**Short term market**
	Complex relationship between power factor, MW output, and heat losses (additional costs)	Need to give the opportunity for participants to bid portions of capacity to reflect non-linear cost	**ST market, availability and utilisation fee (or volume visibility)**
	Poor visibility over dispatch commitments	Dispatch risk should sit with ESO (to the extent possible), availability only fee requires participant to forecast dispatch and price in	**Both availability and utilisation fee (or volume visibility/cap)**

Figure 2: Commercial barriers in reforming the UK reactive power services market (National Grid ESO, 2019, Reactive Reform - Market Design).

Figure 3: A simplified electrical diagram of the TC-RWP power system.

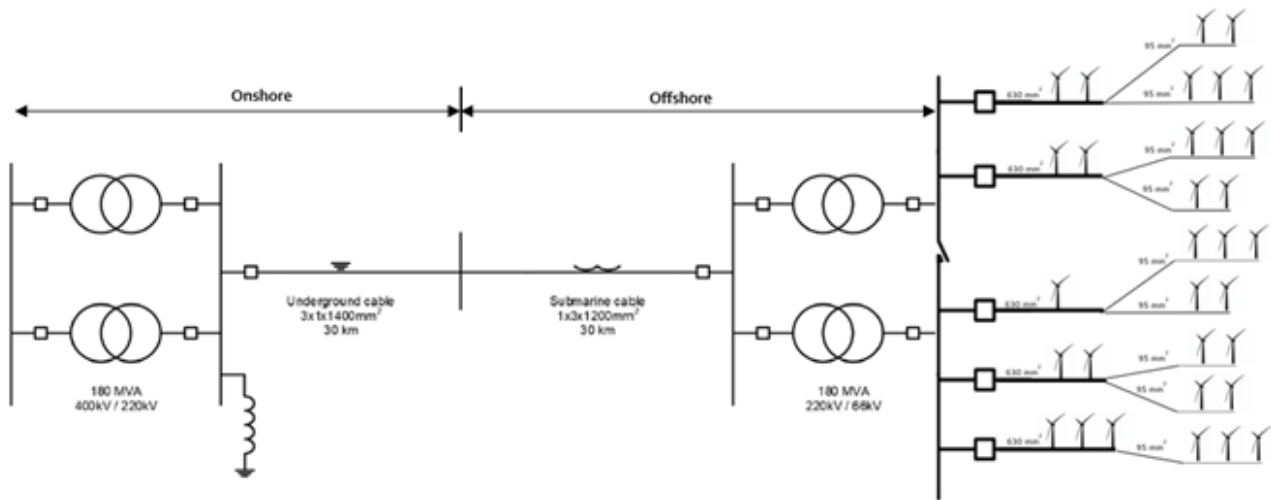Enhanced reactive power service (ERPS): This is suitable for generators who can provide reactive power over and above the Grid Code and ORPS requirements. In such situations, generators are generally instructed to provide a target MVAR level which must be reached within two minutes. In both services, the instructions for reactive power are normally sent from the system operator to the generator via an electronic dispatch logging (EDL) system. Furthermore, the UK is exploring potential solutions to reform the reactive power services market to include other participants such as providers of battery energy storage who can help tackle further challenges related to reactive power and system voltage control. This is currently being explored by National Grid ESO in the project "Future of reactive power" (National Grid ESO, 2019, Reactive Reform - Market Design). Some of the highlighted commercial barriers are summarised in Figure 2.

2.2 Power system design

The electrical layout of the TC-RWP has been conducted according to the EERA DTOC inter-array design procedure (Endegnanew *et al.* 2013). The inter-array grid voltage is 66 kV, which is foreseen as the standard for the next generation of offshore wind farms, with turbines now within the 10 MW rating. It consists of two strings of 7 turbines, and three strings of 6 turbines as shown in Figure 3. Further information of the electrical characteristics of the network are summarised in Merz *et al.* 2019, and TotalControl Deliverable D4.2.

2.2.1 Wind farm layout design

The wind farm layout design for the TC-RWP is presented in Merz *et al.* 2019 and TotalControl Deliverable D4.2. This consists of 32 turbines in a staggered pattern with the separation between rows and columns 5 times the rotor diameter i.e. 5D (D = 198 m). Hence considering the spatial locations, the length of the cable sections between individual adjacent turbines is either 0.99 km (5D) or 1.1 km (5.6D) as shown in Figure 4.

2.2.2 Collector grid cable design

The cable model is a representation of the XPLE 3-Core aluminium submarine cable. The thick and thin lines represent different cable types whose properties are summarised in (Merz *et al.* 2019). The chosen cross-sections 95 mm2 and 630 mm2 are used based on the current rating.
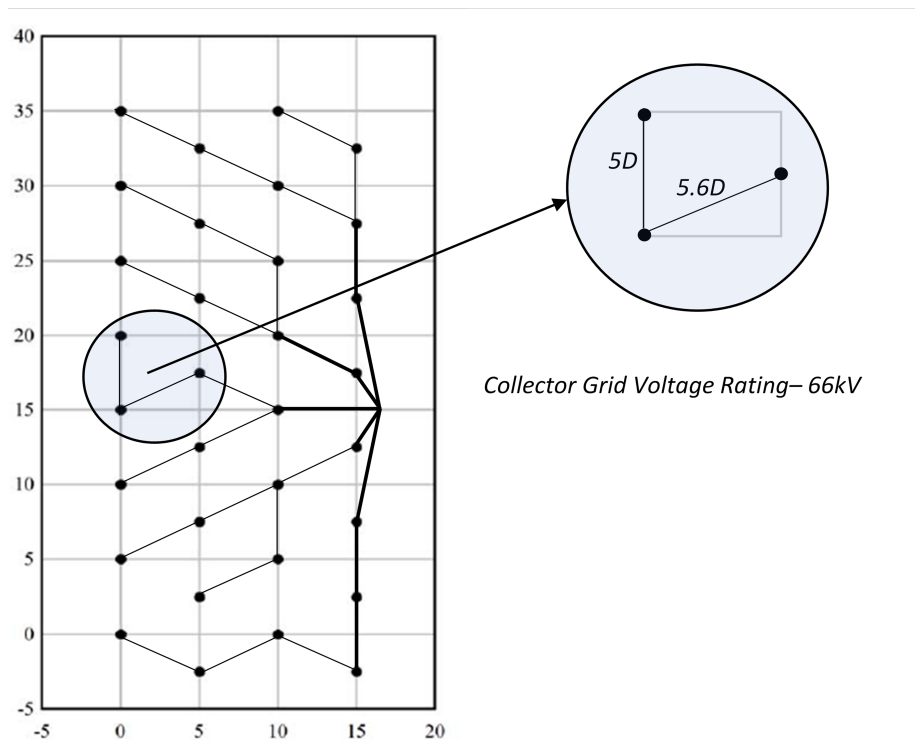
PROJECT
TotalControl

REPORT NUMBER
D4.6

VERSION
1.0

8 of 47

Figure 4: Collector grid cable section layout of the TC-RWP (D = 198 m).

Within the PSCAD simulation program, there is no sufficient model provided for 3-core XPLE cables. However, there is the flexibility to build such models provided there is detailed sufficient information of the required cable parameters. The PSCAD simulation program provides two approaches to model the cable sections either through the Cable or Transmission line libraries.

- Creating models with the Cable library: The choice for this approach depends on the complexity of the system under study. For example, the cable library representation provides a model with a detailed description of the cable parameters such as cable formation (i.e. flat or trefoil), distance between conductors, laying depth conductor diameter, soil temperature, cable propagations etc. and would suit the sort of system analysis for studying complex cable designs.

- Creating models with the Transmission line library: This approach captures mainly the frequency response characteristics of the cable and suits analyses where the focus is on the resistance and reactance values of cables (i.e. R, Xc, Xl). Three types of transmission line models are provided depending on the complexity

1. Pi-Section Model: This is appropriate for system studies that are based on a single frequency but does not capture travelling waves within cables. An example use case are grid system studies at 50 Hz.

2. Bergeron Model: This is also appropriate for single frequencies and in addition captures travelling waves.

3. Frequency dependent model: This captures a wider range of frequencies DC up to GHz and also reflections.

In this system study, most of the analysis undertaken builds on wind farm control and how it interacts with the active and reactive power requirements (PQ) of the network. Hence, the pi-section

PROJECT
TotalControl

REPORT NUMBER
D4.6

VERSION
1.0

9 of 47

Parameters	Values
Resistance	2.46e-4 (Ω/m)
Inductive Reactance	1.33e-4 (Ω/m)
Capacitive Reactance	18.7241 (MΩ*m)

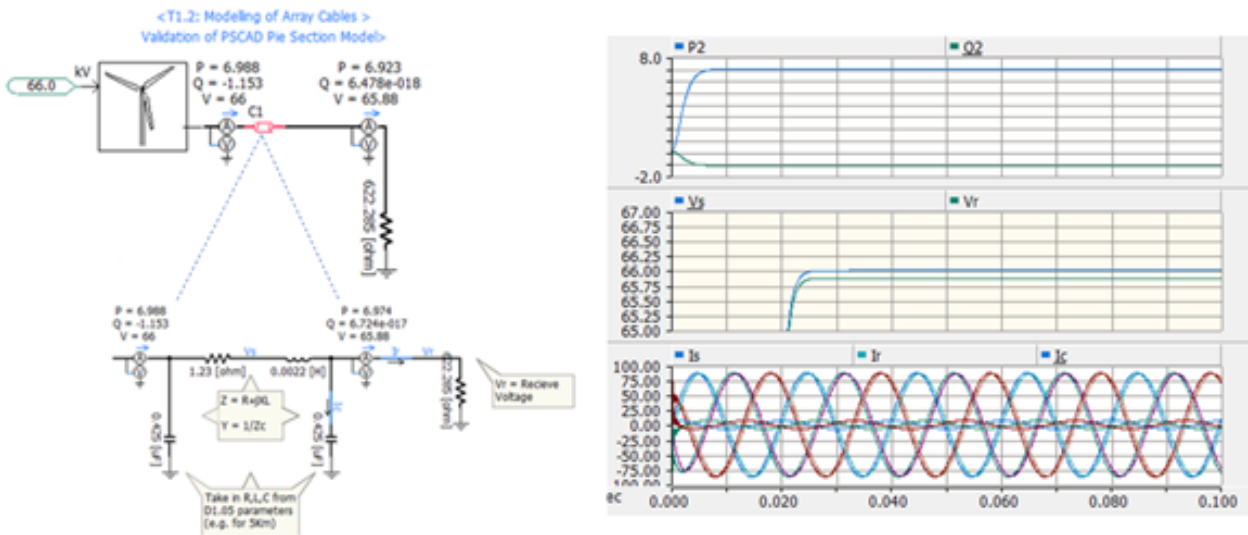*Table II: Collector grid pi-section cable parameters.*

Figure 5: Cable pi-section PSCAD model validation.

equivalent model is sufficient to represent the design of the 0.99 km and 1.1 km cable sections. Table II summarises the properties of pi-sections based on the RLC cable parameters provided in (Merz *et al.* 2019).

Design validation for reactive power:

For both 0.99 km and 1.1 km long cables, the reactive power of the pi-section was validated. In the example, the reactive power Q for a 5 km length of cable is -3.142 x |66 kV| x (0.245 µF) = -1.16 MVAR. This is shown the PSCAD pi-section model in Figure 5.

2.2.3 Sub sea and land export cable design

A description of the export system is presented Figure 3 showing the layout from the onshore to offshore connection points. Table II in (Merz *et al.* 2019) lists properties of the submarine collection grid cables, as well as the export cables over the submarine and land sections. The PSCAD simulation program presents a high-fidelity representation of the expert system with detailed model of a 180 MVA transformer and high voltage AC export cable. In the transformer model, the core non-linearity is represented with non-linear characteristics approximated based on the 'knee point', the 'air core reactance' and the magnetizing current at the rated voltage.

Similar to the approach taken in section 2.2.2, the transmission line representation was used to model the underground and submarine cables each 30 km in length. Here, the Bergeron model was chosen as this is good enough representation for most power system studies using the details of cable characteristics are presented in (Merz *et al.* 2019).

For the shunt reactor, this is placed by the 400kV/220kV onshore transformer substation, and it compensates 100% of both cables' reactive power. The is modelled based the description of the X/R ratio of 500 provided. The system is modelled to be grid connected, with the point of connection

PROJECT
TotalControl

REPORT NUMBER
D4.6

VERSION
1.0

10 of 47

(PoC) being at the onshore substation.

2.3 Wind turbine control architecture

The detailed model design for wind turbine controller has been described in the Total Control Deliverable 4.2 (Merz *et al.* 2019). The optimal dispatch operation of large wind farms whilst minimising reactive losses will further reduce the power losses of the wind farm increasing the annual yield. In the current the approach, the system operator (SO) dictates the changes to the setpoints control described in Table I (i.e. reactive power, power factor or voltage control) for reactive power support. In such situations, the grid code compliance and network connection agreements from the SO have to be fulfilled and it is up to the control principles of the wind farm control which relies on the coordination of the wind turbine controllers of the wind turbines in the wind farm.

2.3.1 Requirements and priorities between wind turbines and substation

With regards to the requirements and priorities between the wind turbines and substation, the wind turbine controller is responsible for properly operating and distributing relevant data coming from the following sources:

System Operator (SO): This is the dispatch centre and commands are sent to the wind farm controller (WFC) from the SO regarding GCC under normal operation conditions and reactive power support during frequency or voltage events. These commands are sent to the wind turbine controller via the WFC and are used to respond to corresponding reactive power supply set points.

Offshore Substation: The measurements form the reactive power parameters such as the power factor, voltage, active and reactive power at the point of connection (PoC) to the offshore substation should ideally form a closed loop control in the wind turbine controller when compared from the SO to meet the set point control requested.

Both priorities described above must be met by the wind turbine controller in order to comply with the GCC.

2.3.2 Requirements and priorities at each wind turbine

With regards to the requirements and priorities at each wind turbines, the wind turbine controller is responsible for measuring time critical measurement signals locally and transferring these measurements to the corresponding control systems responsible for wind flow and electrical dynamics of each turbine. These include the following systems:

Energy Capture and Power Production: This captures the energy generated from the wind flow dynamics of the turbines by regulating subsystems controllers such as the pitch, yaw, generator torque and converter. This works to ensure the highest efficiency of operation that maximises the power extraction under varying wind conditions whilst ensuring safe operation.

Load Reduction: This ensures that the wind turbine loads are kept within their design envelopes and avoids high load conditions which could cause excessive wear of structural components. This could also include load reduction strategies, but this must not affect the overall operation of the turbine and comply with grid code requirements described in Section 2.1.

Safety and Protection: This triggers safety controls and procedures in situations where each turbine need to protect itself from adverse conditions such as grid faults. The wind turbines controller must be able to detect signals related to ensuring the safety of each the turbine.

2.4 Wind farm control architecture

Traditionally, WFC (wind farm control) focused on the grid connection properties of the wind farm to fulfil grid code requirements and/or sell ancillary services. This control focus is referred to as WF-GC (Wind Farm Grid Control) as suggested in Deliverable 4.7 (Hille *et al.* 2020). An example of today's
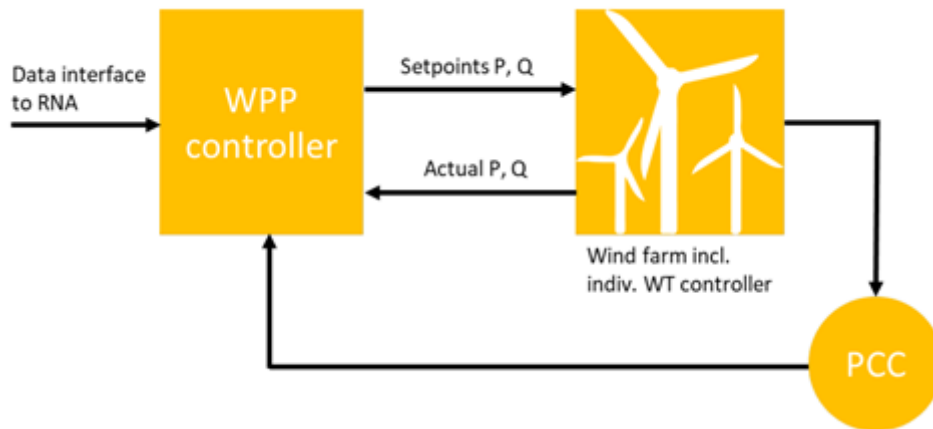
Figure 6: State-of-the-art WF-GC (Source: FarmConners Report D2.1). PCC, point of common coupling, equals the PoC.

state of the art WF-GC is given in Figure 6 (source: FarmConners report D2.1). The WF-GC is here called wind power plant (WPP) controller.

In recent times, WFC is extending to additionally cover optimising the overall performance of the wind flow dynamics of the wind farm by implementing advanced control systems such as axial induction control, wake steering and wake mixing. This control focus is referred to as WF-FC (Wind Farm Flow Control).

For implementing WF-GC into the complete WFC, co-operation with WF-FC is necessary. The following approach is suggested in Figure 7 as part of the developments in the Total Control Deliverable 4.7 (Hille *et al.* 2020).

Here, the set point control signal is from the SO which could be based on reactive power grid support. Within the figure, the WFC is highlighted in a box, showing the general software functionality of the WFC to perform a kind of grid-based case selection. The case selection will be "normal operation" if the request from the SO is not related to a fault in the electric power system outside the wind farm. The Wind Farm Flow control (WF-FC) is also shown to handle the wind flow conditions whilst the Wind Farm Grid control focuses more on electrical system events such as grid faults.

This approach requires a switch-over between two states within the WFC:

1. Normal operation with no grid failure means operation of WF-FC and WF-GC

2. Grid fault operation means switch-over to WF-GC only and to de-activate WF-FC during fault duration

Due to that fact, the system operator (SO) in charge is allowed to require limiting reactive power change rates in one or the other way. No other control feature, e.g., WF-FC should be allowed to change the reactive power in a contradictory way compared to those ramp rates or other limitations of reactive power required by the grid code. Hence, it is important that the WFC is able to understand and distinguish clearly when these scenarios happen unless there is a clear understanding of the behaviour of WF-FC strategies like wake steering in these situations and how they would adhere to maintaining the system requirements of the grid code.

2.4.1 System challenges at wind farm and substation

Wind Farm and Wind Turbine Synchronization: There are challenges, such as how to synchronize the response of the controlled devices, which are spread over large distances. As an example, the voltage control in large wind farms is governed by two distributed controllers: local voltage control at the
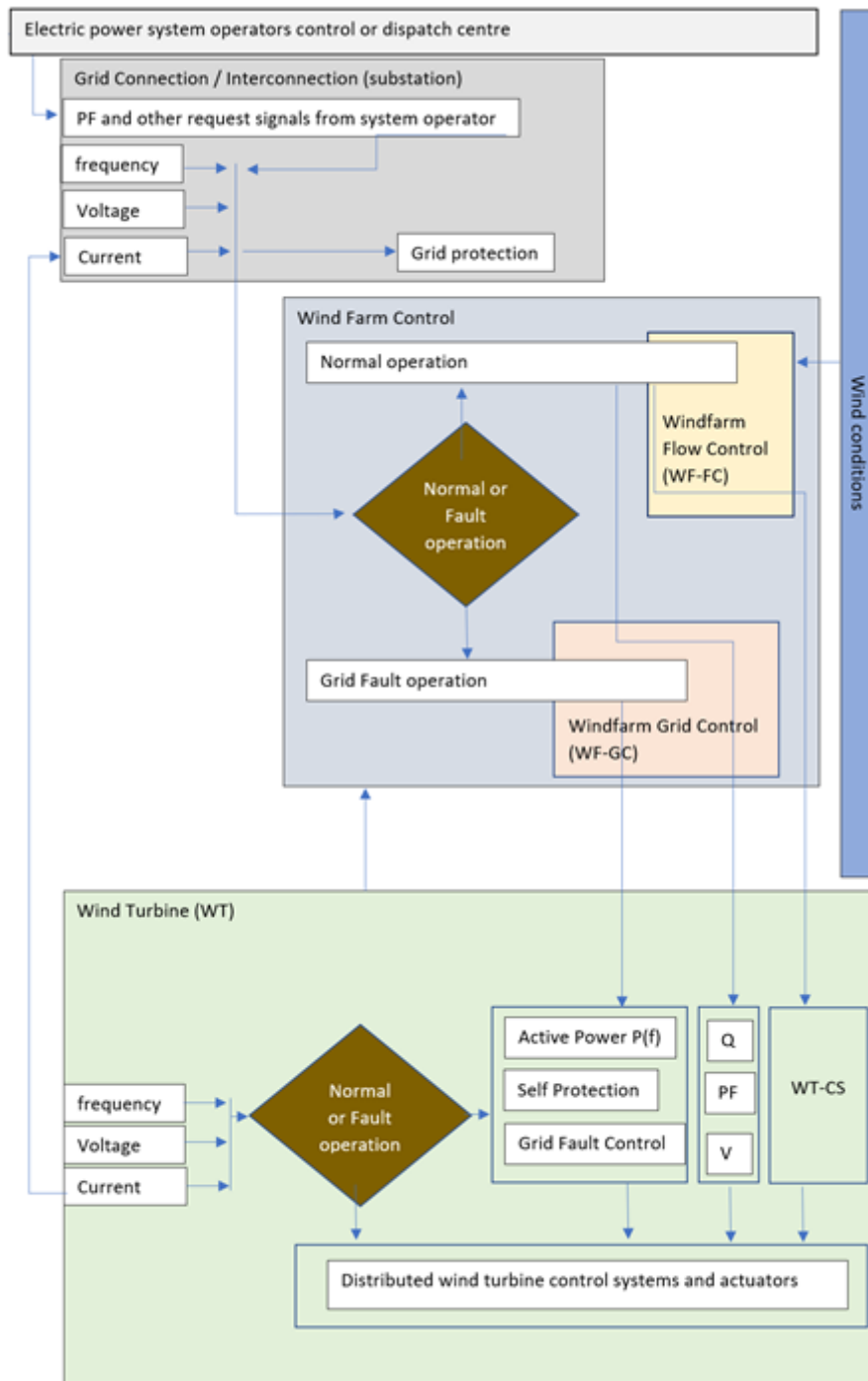
PROJECT
TotalControl

REPORT NUMBER
D4.6

VERSION
1.0

12 of 47

Figure 7: Priority co-ordination regarding wind farm control (WFC) (Hille et al. 2020).

wind turbine terminals combined with overall wind farm voltage control at the Point of Connection (PoC) using a STATCOM.

Reactive Power Losses between PoC and Substation: Practical experience has shown that the design of the voltage and/or reactive power control loops – both at wind turbine and at wind farm level – is crucial in avoiding reactive power oscillations at the PoC that can, ultimately, lead to voltage instabilities in the wind farm collector grid. This is part of the recommendations put forward in the Total Control Deliverable D4.7 (Hille *et al.* 2020) as shown in Figure 7 with reactive current signal path which is better for reducing overall losses in the wind farm due to reactive power currents.

2.5   Wake steering power system model

The electrical power system model for the Total Control Reference wind power plant has been modelled in detail in previous deliverables as described earlier. This provides information for the electrical representation of the layout for the collector grid with cable sections and of the high voltage 220 kV AC export system. The model is built on PSCAD simulation software which is suitable for this sort of analysis as it captures non-linear high frequency oscillation events and more real-life representations than other power systems packages in MATLAB which are better suited for building complex controllers. The wind farm layout is as described in Section 2.2.1 and consists of 32 wind turbines rated at 10 MW following the DTU reference wind turbine detailed in D1.03 (Andersen *et al.* 2018). Each turbine has its own wind turbine controller able to control individually the power setpoints from SO through a WFC. Compensation for the export cable is based on using the passive compensation requirements detailed in D1.5 (Merz *et al.* 2019).

Wake steering is performed by yawing selected wind turbines away from the optimal alignment with the wind direction. This is a wind farm flow control (WF-FC) technique used to optimise the direction of the wake behind the turbines. This allows other wind turbines located in the downwind to increase their energy yield, because the wake is steered away from them. The yaw angle of a wind turbine relative to the incoming wind direction plays a significant role in power production and the yaw misalignment of some of the upstream turbines increases the energy yield from the wind farm.

2.5.1   Wake steering wind farm layout design

The wake steering power model is based on an extension of high-fidelity simulations performed as part of the Total Control project (Andersen *et al.* 2018) by DTU as shown in Figure 8. This is the same as that in Section 2.2.1 but provides more details on the position of the turbines and the wind direction within the wind farm. Large eddy simulations (LES) were performed for different atmospheric conditions and wind directions, and a subset of the data is publicly available (Andersen *et al.* 2020). The selected case corresponds to a conventionally neutral boundary layer with a geostrophic wind of G = 12 m/s, a roughness length of z0 = 2×10−3 m, and a Coriolis parameter of fc = 10−4 s-1, which 995 represents a latitude of 43.43, see additional details in (Andersen *et al.* 2019). The resulting mean wind velocity at hub height is approximately 10.4 m/s.

This layout has been adapted in the PSCAD electrical power system model described earlier in Section 2.2. Figure 9 shows the adopted layout for this design in PSCAD using the same position of the turbines and the wind direction within the wind farm. Figure 10 shows an overview of the wind farm design developed in the PSCAD simulation software.

2.5.2   Power gain/loss under single wake

An additional simulation was performed for the TC-RWP as part of blind tests in the FarmConners project (Göçmen *et al.* 2022). Here, WT32, WT29 were selected as the upstream turbines with corresponding downstream turbines being WT28, WT25 as shown in Figure 8. The upstream turbines WT32 and WT29 are misaligned for 20°and 30°counter-clockwise, respectively and the power gains

PROJECT
TotalControl

REPORT NUMBER
D4.6

VERSION
1.0

14 of 47
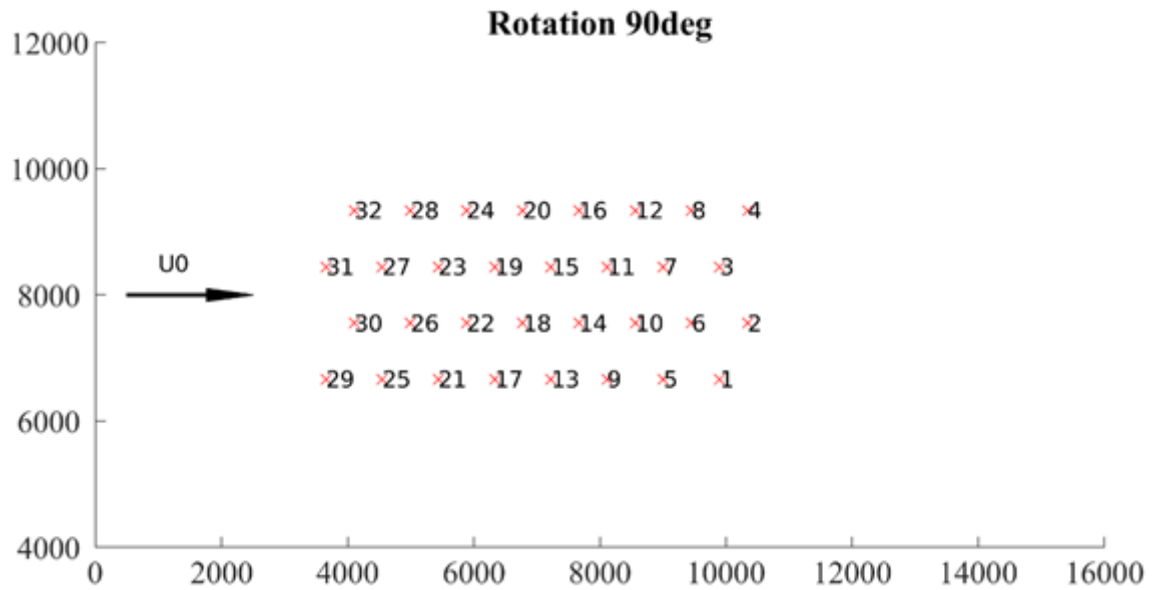
Figure 8: Layut of the TC-RWP with wind direction. The turbine IDs are referred as WT1, WT2, ..., WT32 throughout the rest of the part one.

Layout of Total Control Reference Wind Power Plant. Axis have units s/D, that is, length in terms of rotor diameters, where D=198m

Thin black lines: Cable area 95 mm2, ampacity(1) 300 A. Thin black lines: 150 mm2, 375 A. Thick black lines: 500 mm2, 655 A
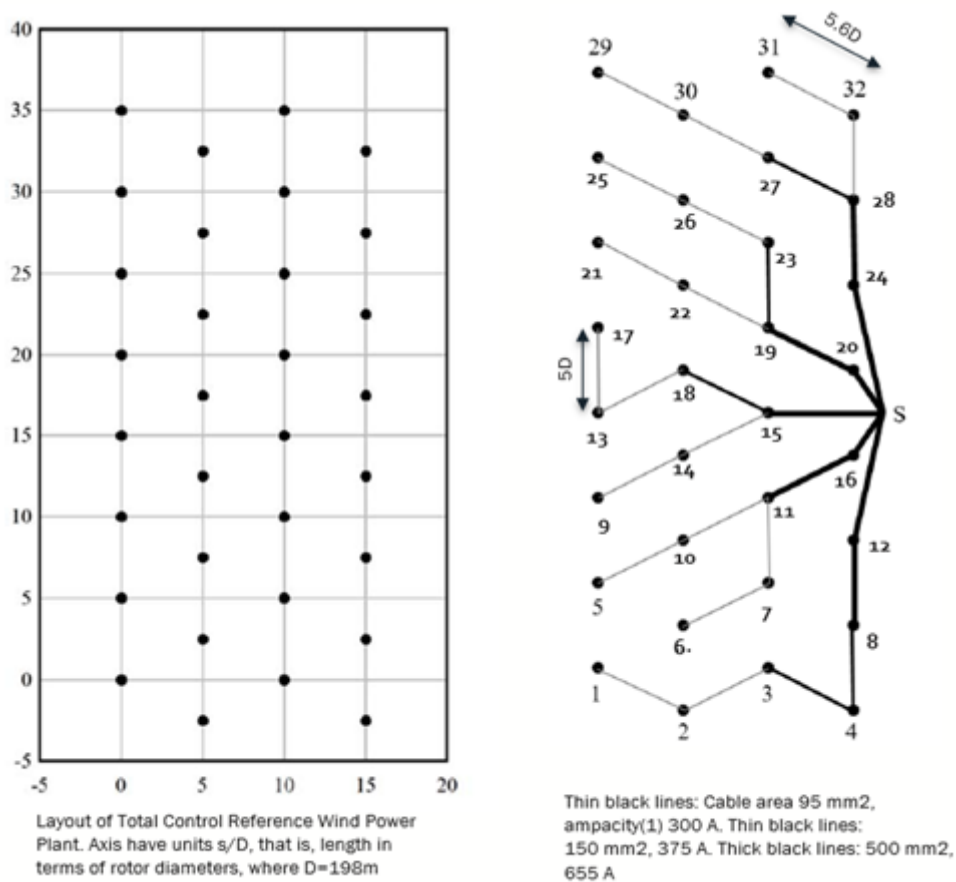
Figure 9: Adopted layout and position of wind turbines in the wind farm.

PROJECT
TotalControl

REPORT NUMBER
D4.6

VERSION
1.0

15 of 47

Figure 10: Representation of the wake model TC-RWP power system in PSCAD.
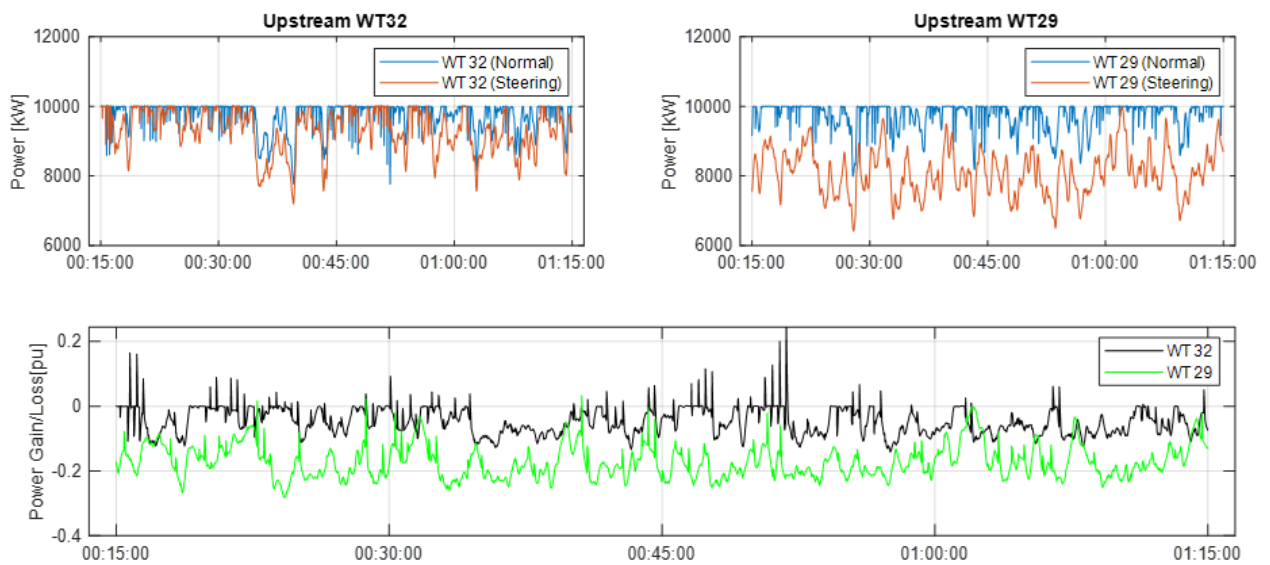
Figure 11: TotalControl LES blind tests, estimated power loss under single wake steering for WT32 misaligned by 20°and WT29 misaligned by 30°.
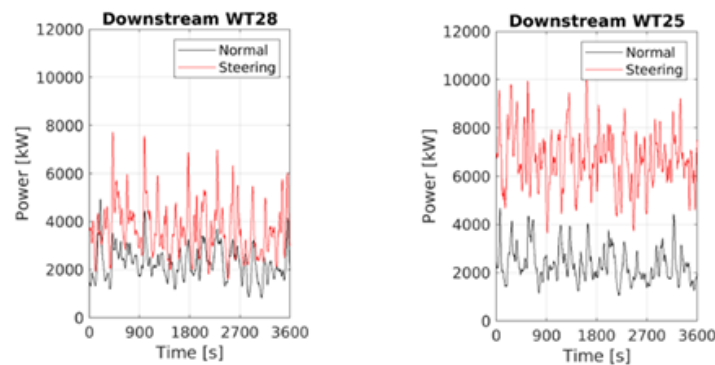
Figure 12: Power time series for single-wake scenario in the TotalControl LES blind test for downstream turbines WT28 and WT25.

are calculated within a 1-hour simulation window. Figure 11 shows the power losses in WT 32 and WT29 when their yaw angles were misaligned.

By intentionally yawing the upstream turbines, at a corresponding wind direction of 90°, the power production during normal operation (in black) and when steering was introduced (in blue) shows an increase downstream as expected and a reduction in power production at the upstream turbine. This is illustrated as shown in the Figure 11. This shows at any point in time a power loss and gain anywhere within the region of approximately 20%.

Figure 12 shows the power gains at the downstream turbines (WT28 and WT25) from the studies in the FarmConners Benchmark Blind test (Göçmen *et al.* 2022). In the trend, we notice the power production of the downstream turbine is increased as expected when steering is applied. This shows an additional power gain of u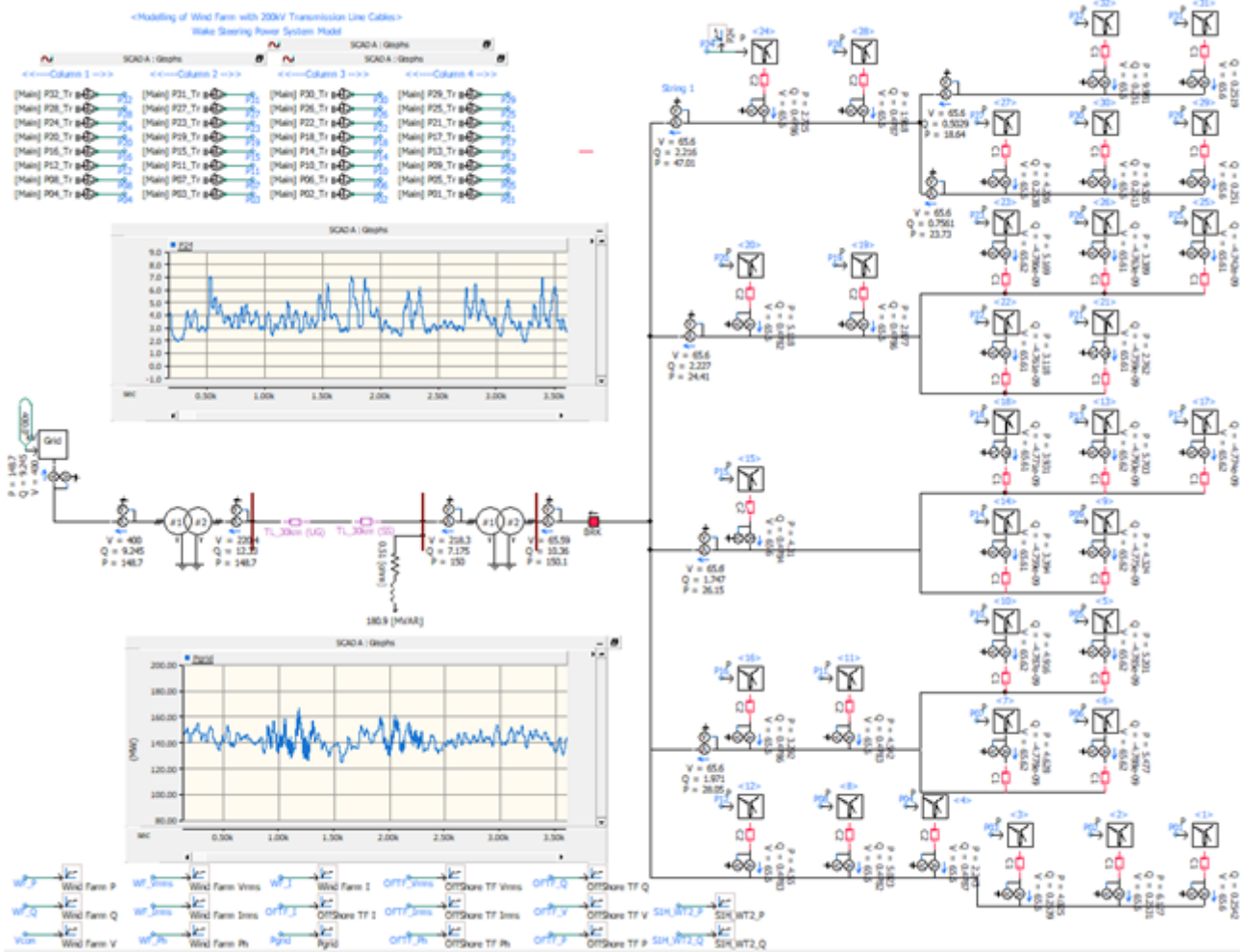p to 150% at any point of time compared to normal operating conditions. The maximum yaw misalignment of 30°(WT 25) is also shown to provide the most energy yield. This thus shows the importance of wake steering in improving power production between upstream and downstream turbine pairs in a wind farm.

2.5.3   Power gain/loss under multiple wake

In order to demonstrate the performance of farm flow control within wind farm control technology, the FarmConners project launched a common benchmark for wind farm flow control code comparison (Göçmen *et al.* 2020). This unique database combines the efforts of the connected WFC projects of different sizes all over Europe and the TotalControl wind power plant under study in this deliverable. As part of these activites, different blind tests were undertaken with 13 participants submitting the results from their models to assess the WFC methods.

The multiple wake scenario considers all the turbines in the wind farm. In this case, 8-turbine subsets with 5D spacing within the TotalControl reference wind power plant are analysed, namely the vertical columns WT32, WT28, ..., WT4 and WT29, WT25, ..., WT1 in Figure 9. Similar to the single wake cases, 20°and 30°counter-clockwise upstream yaw misalignment control scenarios for 90°incoming wind direction are investigated for the multiple wake results in TotalControl LES blind tests. Due to the unavailability of datasets for each turbine required for a comprehensive study in this scenario, the resulting views from the TotalControl LES Blind test from the FarmConners project benchmark tests (Göçmen *et al.* 2022) are used to investigate wake steering reactive power studies in the next section. In the FarmConners benchmark, the median trend shows positive power gains of up to 30% across the whole wind farm. This resulting range is used to validate the subsequent normal operation data for reactive power for the whole wind farm in the next section.
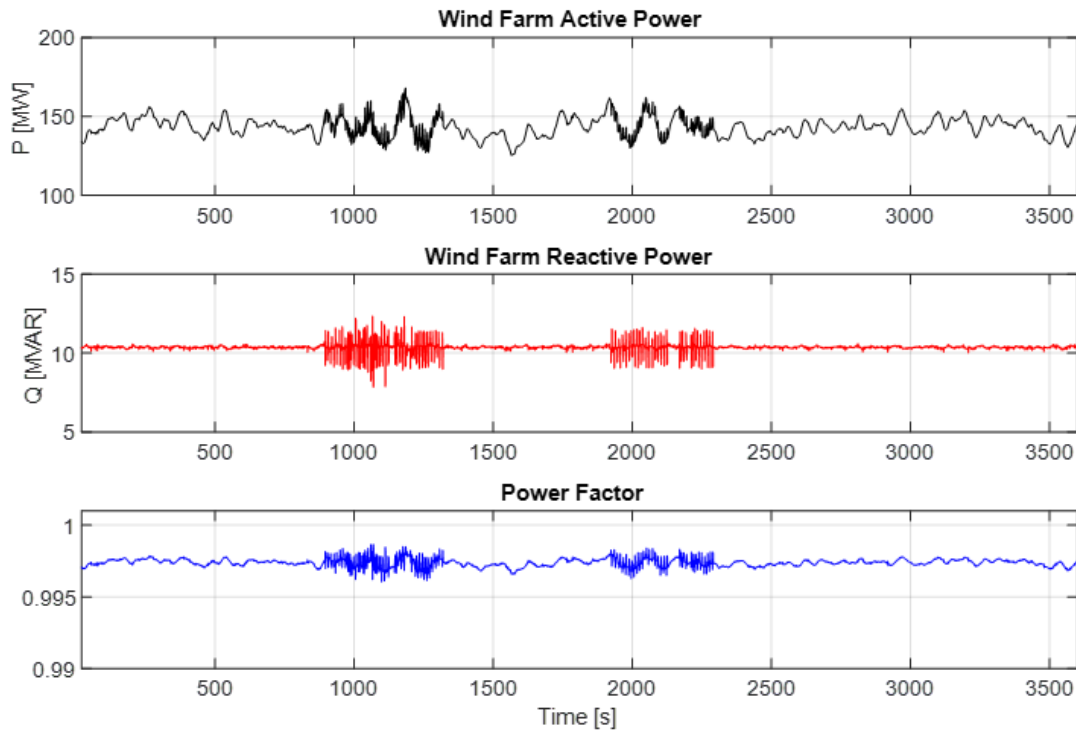
PROJECT
TotalControl

REPORT NUMBER
D4.6

VERSION
1.0

17 of 47

Figure 13: TC-RWP reactive power and reactive power factor under normal operation.

2.5.4 Reactive power studies – wake steering

Existing design rules assume that Wind Turbines (WTs) are aligned to the wind direction throughout their entire operational life. Most WTs are designed to stay online (generator connected to the grid) for some time in defined grid disturbances (fault conditions of the electrical grid) or when the System Operator (SO) requires additional grid support. In such situations, they need to contribute to grid stability by delivering defined amounts of reactive power. Grid conditions (like e.g., voltage) may change very fast and WTs need to perform fast control actions to stay online. These actions are tuned for ordinary alignment to the wind and there is a risk that their safety system shuts the turbines down if a grid disturbance occurs at times of large yaw misalignments. Hence, when introducing or optimising WF-FC features in a wind farm, close attention must be paid that the wind turbines (WTs) are not operated outside their allowable GCC P-Q envelope.

Based on the wake steering power system model developed in section 2.5.1, the following reactive power studies were performed to investigate how compliant the wind turbines are under wake steering. A similar approach can be taken to understand the behaviour of other related wind farm control methods.

Reactive power support – normal operation Figure 13 shows the reactive power for the TC-RWP under normal operation (no steering) and with no reactive power support requested from the system operator (SO). The average capacity factor of the wind farm is 37% during this 1-hour window. With no reactive support request or control, the turbine reactive setpoints are set to zero and only the reactive power of the passive components such as cable sections and transformers are shown in the power network. According to UK grid codes, in order to be grid compliant, the wind farm must be able to keep the limits at any point between 0.85 power factor lagging and 0.95 power factor leading. Here, the design of the TC-RWP is shown to be grid compliant with the power factor between these ranges.
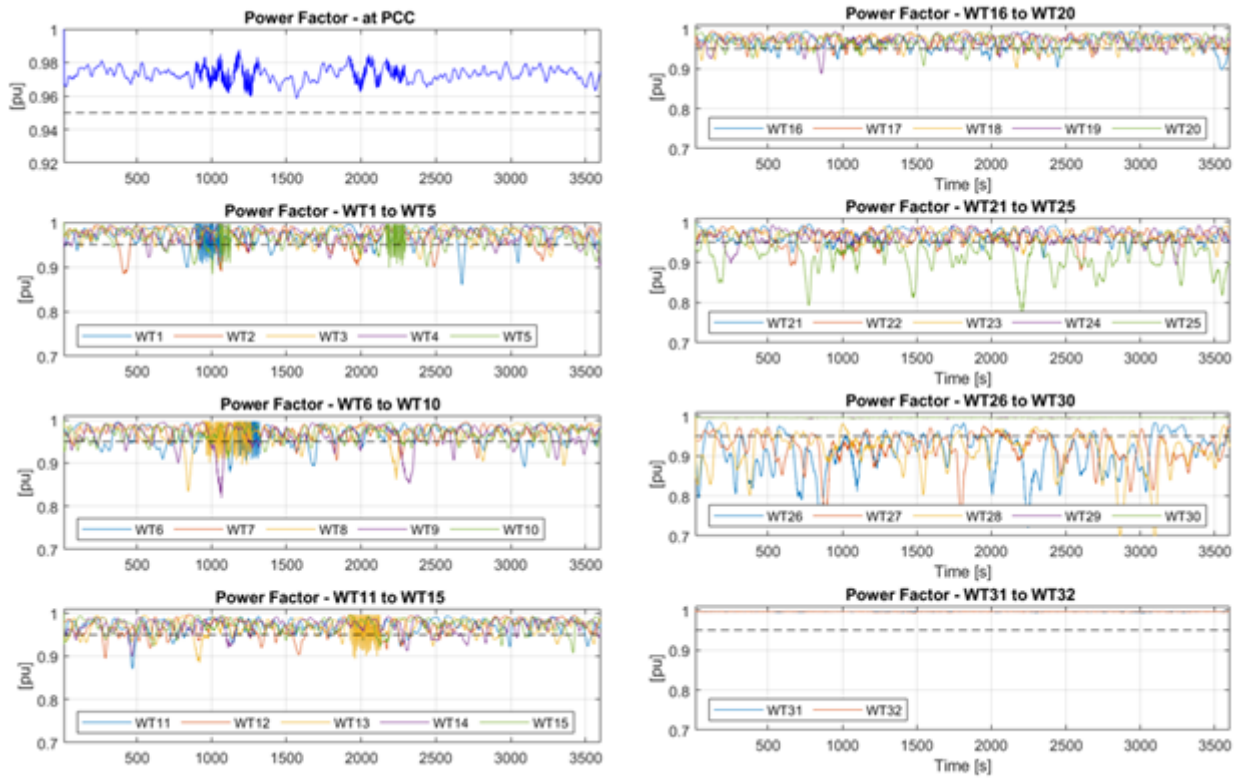
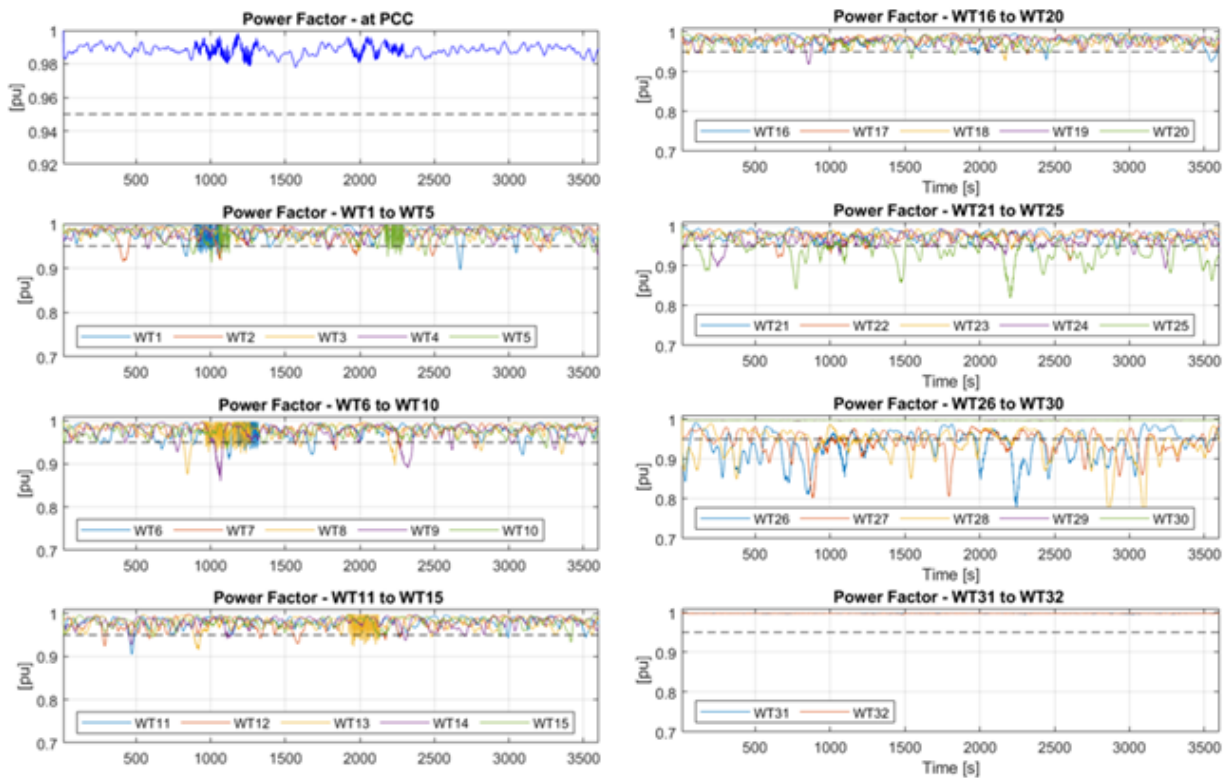*Figure 14: TC-RWP power factor under reactive power support.*

Figure 15: TC-RWP power factor under reactive power support and wake steering.

PROJECT
TotalControl

REPORT NUMBER
D4.6

VERSION
1.0

19 of 47

Reactive power support – wake steering Optimization of reactive power dispatch within large wind farms is described in D2.4 [17]. Taking this into account, the optimal way of reducing electrical losses within the wind farm while the SO is requesting control of power factor will need to include the optimisation principles from D2.4 into the WFC. In such situations, the requirements (regarding power factor or reactive power) from the SO have to be fulfilled. It is up to the WFC which of the WTs within the wind farm will deliver (or consume) the corresponding reactive power whilst keeping in line with the design of their P-Q envelopes.

Figure 14 shows the power factor experienced in the TC-RWP without wake steering as well as the power factor experienced at all 32 wind turbines. This shows results when the system operator (SO) requests 30 MVAr to support the grid. Based on UK grid codes, at the PoC the wind farm is shown to be grid compliant within the 0.95 power factor leading range. Although this meets the conditions from the systems operator, it shows across the 32 turbines the possibility of some WTs operating outside their P-Q envelopes. This is clearly evident in some cases like WT25 – WT28 where the power factor falls frequently to 0.8.

Figure 15 shows the power factor experienced with multiple wake steering and under reactive power support. Here, a maximum power gain of 20% is applied across the wind farm in line with the results from the FarmConners Total Control LES blind test studies (Göçmen *et al.* 2022). The improvement in power factor is clearly visible due to the increased active power range of the wind farm. This is evident in some of the cases WT25 – WT28 where the power factor variation shows some improvement. The improved power factor is also noticeable at the PoC where the baseline increases from 0.96 to 0.98.

2.6 Recommendations and conclusions

Both results highlight the importance of reactive power control of individual WTs when under reactive power support and wake steering conditions and the need to keep wind turbines operational within their P-Q envelopes. For WFC to be deployed in the future, it is recommended that a clear guide is established to consider some of the following:

- The additional reactive power or power factor range that is achievable with optimisation of the reactive power control and coordinated operation of all turbines in a wind farm. The results in D2.4 [17] suggest above 6% improvement in losses with optimal reactive power control alone.

- The additional reactive power or power factor range that is achievable when multiple wake steering WFC technique is deployed. Studies suggest that this can improve the overall power gain by up to 20% (Göçmen *et al.* 2022).

- The design of the P-Q envelopes of individual turbines by ensuring that the WFC maintains operation within these design limits.

- The provision within the SO control room to allow wind turbines to provide reactive support whilst under wake steering conditions. This should provide some flexibility to include opportunities to include wake steering as long as the wind farm is compliant to the grid codes.

- The possibility to use WF-FC but allow to use WF-GC only if there any issue arises during the operation.

3 Coupled dynamics of wind plant with other power plants

3.1 Background

A wind turbine is a flexible structure. Its drivetrain consists of a generator, driveshaft, and aerodynamic rotor, and many wind turbine models also include a gearbox. Fluctuations in the generator air-gap torque – the boundary between the electrical and mechanical systems – can excite resonance in both the turbine's flexible structural components, and in the electric grid. We may therefore expect that under certain scenarios there will be unfavourable electromechanical interactions between the turbine and grid.

Interestingly, there do not seem to be many reports of such resonant interactions associated with existing wind energy installations.[1] At first glance one might assume that the electrical engineers are doing their job: electrical models tend to include a simplified representation of the turbine's first drivetrain torsional resonant mode, and if the frequency response characteristics of this mode are properly calibrated, perhaps problems can be avoided. Yet, this argument is not entirely satisfying, for several reasons:

- Wind turbines are becoming ever larger and in some sense "more flexible," such that the stiffness and frequencies associated with higher drivetrain modes are decreasing.

- Wind power plants constitute a larger fraction of the power generation on the grid, the resonant properties of the turbines can be expected to play a larger role in the grid dynamics overall.

- Wind turbines and power plants rely more and more on advanced controls to achieve acceptable performance, from the perspectives of increasing production, reducing fatigue and extreme loads on the structures, and providing grid support services in order to meet grid-connection requirements. At the same time, the control of the electric grid is also becoming more sophisticated, and there will be a tendency to push the acceptable limits of grid stability in order to incorporate the maximum possible fraction of renewable energy sources. Many of these control functions overlap in frequency band, and there will inevitably be competition for priority, as well as the possibility of unforeseen interactions.

- There is an increasing tendency to place wind power plants farther from load centers, whether on land or offshore, and both the costs and issues with social acceptance of new transmission lines will require the capacity of existing lines to be pushed to the limits. This can result in "weak-grid" scenarios with stronger subsynchronous resonant modes.

We investigate the coupled dynamics of wind turbines and the electric grid, using a proper aero-servo-elastic model of the wind turbine. The electrical components in the wind turbine drivetrain, namely the generator, converter, and transformer, are also represented with a refined model, including the low-level voltage and current controls that end up governing the timescale of the response.

A wind power plant (Section 3.2), thermal power plant (Section 3.7), and hydroelectric power plant (Section 3.8) are connected at a common bus that feeds either a strong grid (Section 3.11) or an isolated load (Section 3.12).

3.2 Characterizing the wind power plant

The wind power plant consists of wind turbines, a collection grid, and a plant power dispatch controller.

---

[1]There are many cases where unfavourable torsional resonance has been encountered, but this has historically been associated with the rotor and drivetrain resonating against the electrical stiffness of the generator, not the wider grid dynamics.
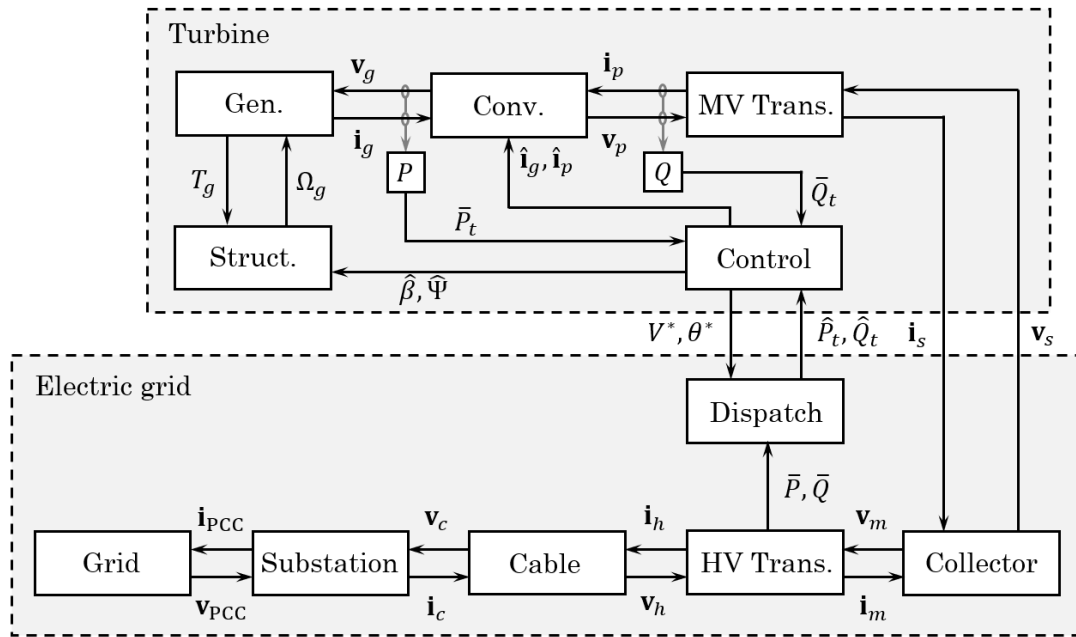
Figure 16: A high-level block diagram of a wind turbine and the grid to which it is connected.

3.3 Wind turbine

The wind turbine is modelled as described by Merz (2018, 2019a, 2019b, 2020), Merz and Pedersen (2018), and Merz *et al.* (2019). The model includes a multibody aeroelastic representation of the structures; an equivalent circuit model of the turbine's generator, converter, and transformer, including low-level voltage and current controls; time-lag models of the pitch and yaw actuators including elastic flexibility and rate saturation; and a wind turbine controller providing rotor speed control, power command tracking, and active tower damping.

We draw the boundary between the wind turbine and the rest of the electric grid at the transformer high-voltage terminals, Fig. 16. Signals passed between the electric grid and the wind turbine must pass through either these terminals, or the wind plant operator's active and reactive power commands, which are sent from the wind plant power-dispatch controller to the turbine controller. Therefore, in relation to electromechanical interactions, we are interested in five input signals: ω_e, $(v_s^\theta)_d$, $(v_s^\theta)_q$, $\hat{P}_t$, and $\hat{Q}_t$, respectively the grid frequency, the d-axis and q-axis transformer terminal voltages, and the active and reactive power commands.[2]

When two electrical components are connected together, we let one "own" the terminal voltage, and the other the current. Thus the state variables $(i_s^\theta)_d$ and $(i_s^\theta)_q$, the d and q axis currents at the transformer medium-voltage terminals, associated with the transformer's inductance, are considered to be part of the wind turbine and delivered to the grid.[3]

Completing the picture of Fig. 16, the wind plant electrical power is measured at the HV transformer. This, together with estimates of the wind speed V^* and direction θ^* at each turbine, are used by the dispatch controller to determine the appropriate power commands. The wind turbine controller receives the power commands, and executes them, along with other functions, through a current command sent to the generator-side converter $\hat{i}_{g/p}$, as well as blade pitch $\hat{\beta}$ and nacelle yaw

---

[2]We are mainly working with linearized models and do not consider transient electrical fault cases, where an additional collective voltage component, or alternatively the abc frame components, would be required.

[3]As a side note, the converter's DC link separates the AC reference frames on the generator and grid sides. The generator-side d and q axes are defined in relation to the generator's magnetic north pole, while the converter-side d and q axes are defined relative to some reference point in the grid, say, the PCC.

PROJECT
TotalControl

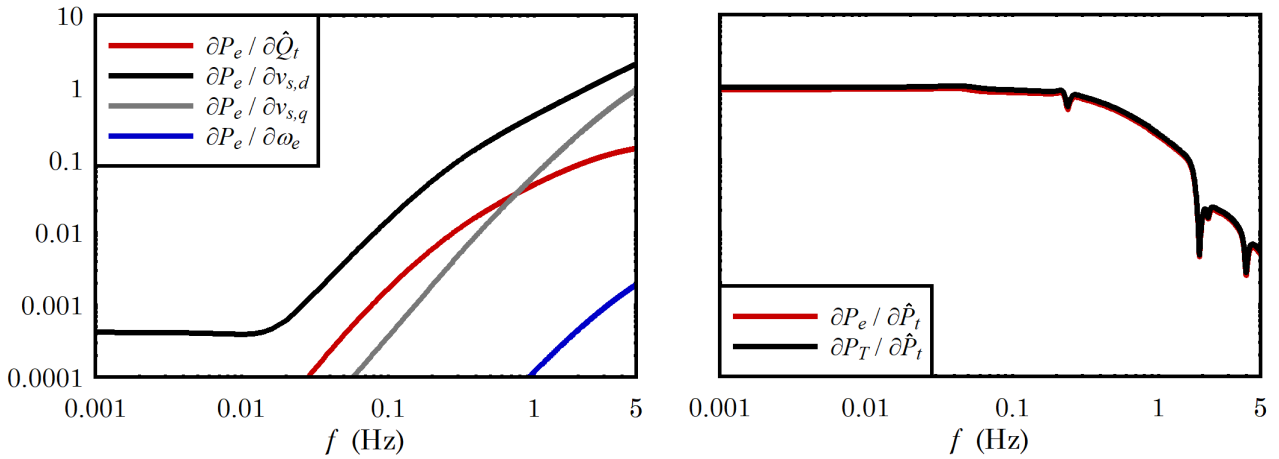REPORT NUMBER
D4.6

VERSION
1.0

22 of 47

Figure 17: Transfer functions between the relevant inputs and the electrical and mechanical (air-gap) output power. Units of voltage are kV, power MW or MVA, and rotor speed rad/s.

$\hat{\Psi}$ commands sent to the actuators.

Let us pick a handful of key metrics representing the turbine's electromechanical response: the terminal power

$$P_s = (v_s^\theta)_d(i_s^\theta)_d + (v_s^\theta)_q(i_s^\theta)_q, \qquad Q_s = (v_s^\theta)_q(i_s^\theta)_d - (v_s^\theta)_d(i_s^\theta)_q; \tag{1}$$

the generator air-gap torque

$$T_g = -\frac{1}{2}n_p\lambda_r^\theta(i_g^\theta)_q; \tag{2}$$

the rotor speed Ω; blade pitch β; nacelle fore-aft and side-to-side displacements d_x^y and d_y^y in the yaw coordinate frame; and blade tip edgewise and flapwise deflections $\delta_{y,0}^\psi$, $\delta_{y,c}^\psi$, $\delta_{y,s}^\psi$, $\delta_{z,0}^\psi$, $\delta_{z,c}^\psi$, and $\delta_{z,s}^\psi$ in the multi-blade coordinate frame. This gives us a collection of 65 transfer functions (5 inputs, 13 outputs) to consider.

Say that a 10 MW wind turbine (Anaya-Lara *et al.* 2018) is operating in a 10 m/s wind and a curtailed power of 6 MW. If the grid voltages or power commands are caused to fluctuate, the responses of the network-side electrical power P_e and mechanical (generator air-gap $T_g\Omega$) power P_T are shown in Fig. 17. When the turbine is isolated and operating without any grid-supporting control functions, as is the case here, perturbations to the active power command $\hat{Q}_t$, grid voltage v_s, or frequency ω_e are effectively isolated from the generator by the converter's DC link, so we see no response in the generator-side P_T (left-hand plot). The response of the active power P_e is due primarily to the current control (DC link voltage and reactive power) of the network-side converter. On the other hand, an active power command $\hat{P}_t$ influences both P_T and P_e, causing the generator to track the command up to a bandwidth of about 0.2 Hz (right-hand plot). Clearly the electromechanical interactions in a wind power plant will be due to the design and tuning of control functions that perturb the active power commands sent to the turbines.

3.4   Collection and transmission grid

Figure 18 illustrates an offshore wind power plant's electrical collection grid and transmission to shore, connected to a simple Thevenin-equivalent load. Typical values for the electrical parameters are listed in Table III, and are based on an existing electromechanical model of the TotalControl Reference Wind Power Plant (Merz *et al.* 2019). This plant contains 32 turbines; only one is represented graphically in Fig. 18.
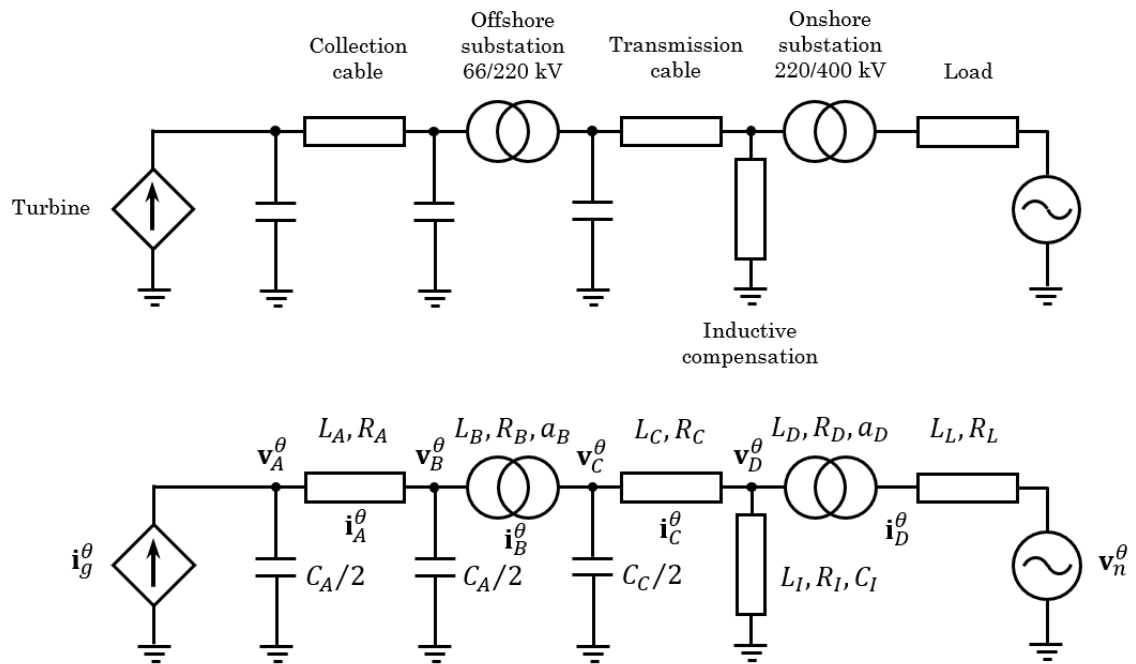
Figure 18: A schematic of the electrical collection grid and transmission connected to a Thevenin-equivalent load.

Table III: Default values of the parameters in Fig. 18.

L_A	9×10^{-4}	H
R_A	0.5	Ω
C_A	2×10^{-10}	F
L_B	4×10^{-4}	H
R_B	0.01	Ω
a_B	0.3	-
L_C	0.026	H
R_C	1.1	Ω
C_C	6×10^{-6}	F
L_I	0.8	H
R_I	0.5	Ω
C_I	6×10^{-6}	F
L_D	0.05	H
R_D	0.01	Ω
a_D	0.55	-

PROJECT
TotalControl

REPORT NUMBER
D4.6

VERSION
1.0

24 of 47

The actual TotalControl wind power plant has a layout where the turbines are connected in strings. The effective properties of the collection grid depend on where the turbine is located along the string; suffice it to say that the values of L_A, R_A, and C_A listed in Table III are approximately those for a "typical" wind turbine in the plant. The overall system properties depend on the load L_L and R_L. If the wind plant is connected to a strong grid, such that L_L and R_L are negligible, then the lowest resonant frequency is around 140 Hz, well above the AC frequency of 50 Hz. The implication is that the dynamics of the baseline wind plant electrical network may be neglected, for purposes of studying sub-synchronous oscillations; the electrical system may be replaced with an equivalent static function, without changing the low-frequency dynamics.

3.5   Wind power plant control

There are broadly speaking two disciplines of wind power plant control: flow control and grid services. Flow control involves adjusting the operating points (rotor thrust/induction, nacelle yaw) in order to adjust the wake effects through the turbine array, typically with the intent of maximizing the plantwide energy capture. This type of control generally acts over long timescales, from the turbine-to-turbine convection time (a minute or two) to the plant convection time (up to a half hour).[4] In the broadest sense there is coupling between the grid and flow, since changing the wind plant's power setting changes the turbine operating points and hence the wake flow. However, due to grid code requirements it is reasonable to assume that the grid support functions – essentially, power command tracking – get priority, especially in the short-term timeframe up to one minute. For purposes of the present analysis we are not concerned with the hourly dynamics of the weather and flow control. Rather, for purposes of modal dynamics we take the wind speed to be a generic input to the system: its mean value determines the operating point, and its perturbation may serve to excite the system; but we do not consider the resulting perturbation to the wake flow through the plant.[5]

Neglecting the plantwide wake flow leaves us with the feedback path from the grid to the turbine structures by way of the active power command $\hat{P}_t$. This comes from the dispatch function (Fig. 16), whose job it is to evaluate the status of the wind power plant and come up with a preferred way in which the total plant command $\hat{P}$ can be met by distributing the commands $\hat{P}_t$ to the individual turbines. Now, the meaning of "preferred" is flexible; it may be a simple strategy, considering only the available power in the wind at each turbine, or it may be something quite complex, based on condition monitoring, turbulence, fatigue rates, forecast winds, lidar measurements, and so on.

As a baseline, we will adopt the hierarchical supervisory control algorithm from Merz *et al.* (2020).[6] This has a simple architecture associated with each wind turbine, Fig. 19, where the objective is to dispatch an appropriate power command $\hat{P}_t$ to the turbine. The algorithm is active under curtailed operation. It attempts to hold the rotor thrust constant on each wind turbine, subject to the requirement that the total plant power is equal to the commanded value. These competing objectives are satisfied by ensuring that the power command tracking function has integral action that in the long-term limit is guaranteed to overrule the thrust compensating function. There are also weighting functions that help properly distribute the thrust compensation to the turbines that need it most: those with the highest fatigue damage rates. The performance is aided by the fact that many turbines act together to produce the total plant power output, whereas the fluctuating thrust due to turbulent winds tends to be weakly correlated from one turbine to another. Further details of the dispatch control algorithm are described in the cited report; suffice it here to focus on the relevant inputs and

---

[4]There are flow-control strategies that involve short-timescale "pulsing" of the rotor thrust (Munters and Meyers 2018). This would either need to be coordinated in a way that limited the overall power fluctuations of the wind power plant, or paired with a short-term energy storage system like batteries to smooth out the fluctuations.

[5]A signal consisting of a perturbation to the flow will diffuse and weaken as it convects downstream; for instance, a step change in the rotor thrust is not experienced as a step change by downstream turbines. Rather, it would appear as a more gradual change in the mean wind speed, and perhaps also a change in the turbulence intensity.

[6]TotalControl Deliverable D4.2

PROJECT
TotalControl

REPORT NUMBER
D4.6

VERSION
1.0

25 of 47
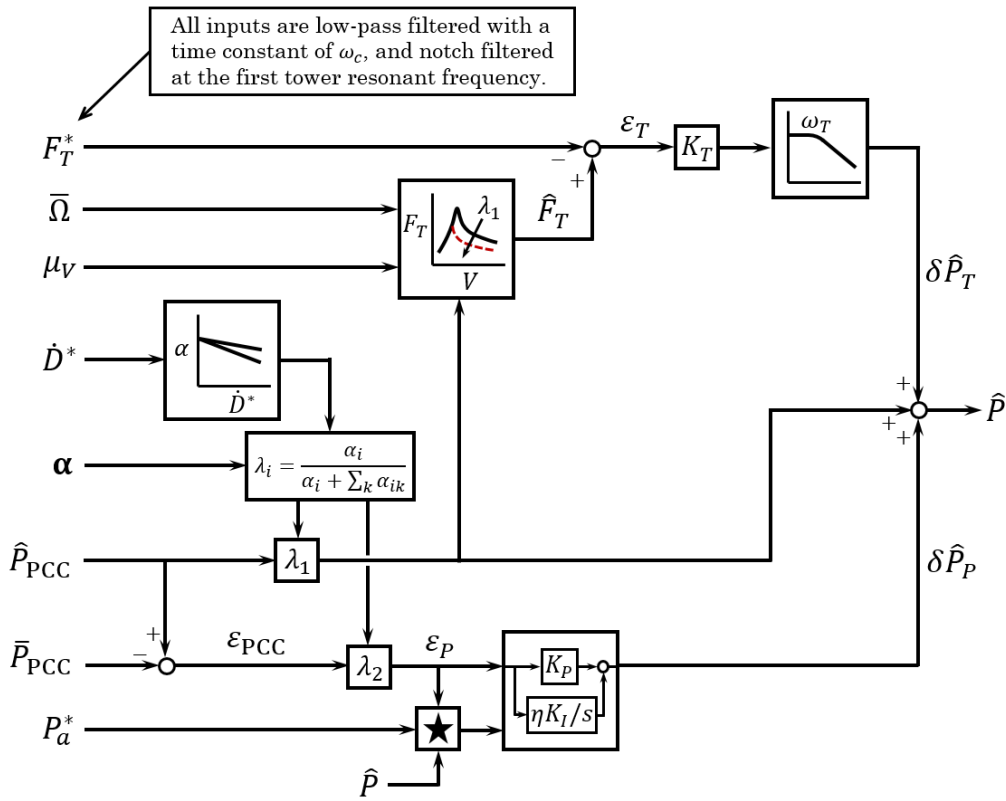
Figure 19: A hierarchical supervisory wind power plant control algorithm, where one of these control blocks is associated with each wind turbine.

outputs.

We shall ignore the inputs for plant-scale wind speed μ_V, estimated turbine damage rate $\dot{D}^*$ and its derived weights α, and the estimated available wind power P_a^*. By "ignore" it is meant that these inputs are considered here to be frozen at their steady-state values and so do not function as dynamic inputs in the linear system model. We are left with four dynamic inputs to the dispatch controller: the estimated rotor thrust F_T^*, which can be computed from a known $C_T(\Omega, \beta, V)$ table; the measured rotor speed $\overline{\Omega}$; the total wind plant power command $\hat{P}_{\mathrm{PCC}}$; and the measured wind plant power $\overline{P}_{\mathrm{PCC}}$. The output from each dispatch control block is the power command $\hat{P}_t$ sent to the associated wind turbine. The links between the dispatch controller and the rest of the system are straightforward: $\hat{P}_{\mathrm{PCC}}$ comes from an external source like the operator or frequency droop control, $\overline{P}_{\mathrm{PCC}}$ is computed from the measured voltage and current at the point of common coupling (PCC), F_T^* and $\overline{\Omega}$ are available as outputs from the turbine model, and $\hat{P}_t$ is an input to the turbine model.

For the present purposes we link the dispatch controller to a frequency-droop controller, which supplies a perturbation in the command $\hat{P}_{\mathrm{PCC}}$ as a function of the grid frequency deviation $\overline{\omega}_e - \hat{\omega}_e$. The droop controller is implemented as a low-pass filter in series with a PI controller,

$$\hat{P}_{\mathrm{PCC}} = \frac{\alpha_\omega}{s + \alpha_\omega} \left[1 - K_P \varepsilon_\omega - \Psi_\omega \right] \hat{P}_{\mathrm{ref}} \tag{3}$$

with

$$\varepsilon_\omega = \overline{\omega}_e - \hat{\omega}_e \tag{4}$$

the frequency error and

$$\Psi_\omega = \int_0^t K_I \varepsilon_\omega \, dt = K_I \frac{\varepsilon_\omega}{s}. \tag{5}$$

PROJECT
TotalControl

REPORT NUMBER
D4.6

VERSION
1.0

26 of 47

Table IV: Default values of the parameters for the dispatch controller.

K_{PP}	1	-	Power command tracking proportional gain
K_{IP}	0.4	1/s	Power command tracking integral gain
K_T	6	m/s	Thrust-balancing control gain
ω_L	0.03	Hz	Thrust-balancing LP filter frequency
α_L	0.08	Hz	Input LP filter frequency
α_n	0.24	Hz	Input tower notch filter frequency
ζ_1	0.04	-	Input tower notch filter damping parameter 1
ζ_2	0.40	-	Input tower notch filter damping parameter 2
α_ω	0.05	Hz	Frequency droop LP filter frequency
K_P	2.048×10^7	Ws/rad	Frequency droop proportional gain
K_I	0	W/rad	Frequency droop integral gain

It is standard to use 20% droop, meaning

$$K_P = \frac{\Delta \hat{P}_{\text{PCC}}}{\Delta \varepsilon_\omega} = 5 \frac{N_t P_r}{\hat{\omega}_e} \tag{6}$$

which in this case gives

$$K_P = 5 \frac{(32)(1 \times 10^7 \,\text{W})}{314.16 \,\text{rad/s}} \approx 5 \,\text{MW s/rad}. \tag{7}$$

The integral gain K_I is adjusted to provide a slow correction, in order to return the long-term frequency to the target value.

Using the baseline parameters listed in Table IV, the response of one of the turbines is shown in Fig. 20. At left is the response to an external operator power command $\hat{P}_{\text{PCC}}$ input to the plant controller, and at right is the response to a fluctuation in the PCC q-axis voltage. The low-frequency asymptote is as expected, with the $\partial \hat{P}_t / \hat{P}_{\text{PCC}}$ sensitivity roughly equal to N_t^{-1}. Noteworthy features in the response are the turbines' rotor speed control mode at about 0.06 Hz, the tower notch filter at 0.24 Hz, and resonant mode associated with the system voltage at about 1.3 Hz. This latter 1.3 Hz mode is of particular interest, and is investigated further in Section 3.10.

For the analyses of Section 3.9, the wind plant is generating 192 MW as a default steady-state operating condition, with each of the 32 wind turbines commanded to provide 6 MW. The wind speed is 10 m/s, and the maximum available power at each turbine is a bit over 7 MW, so the wind plant operates in a curtailed, power-command-tracking mode.

PROJECT
TotalControl
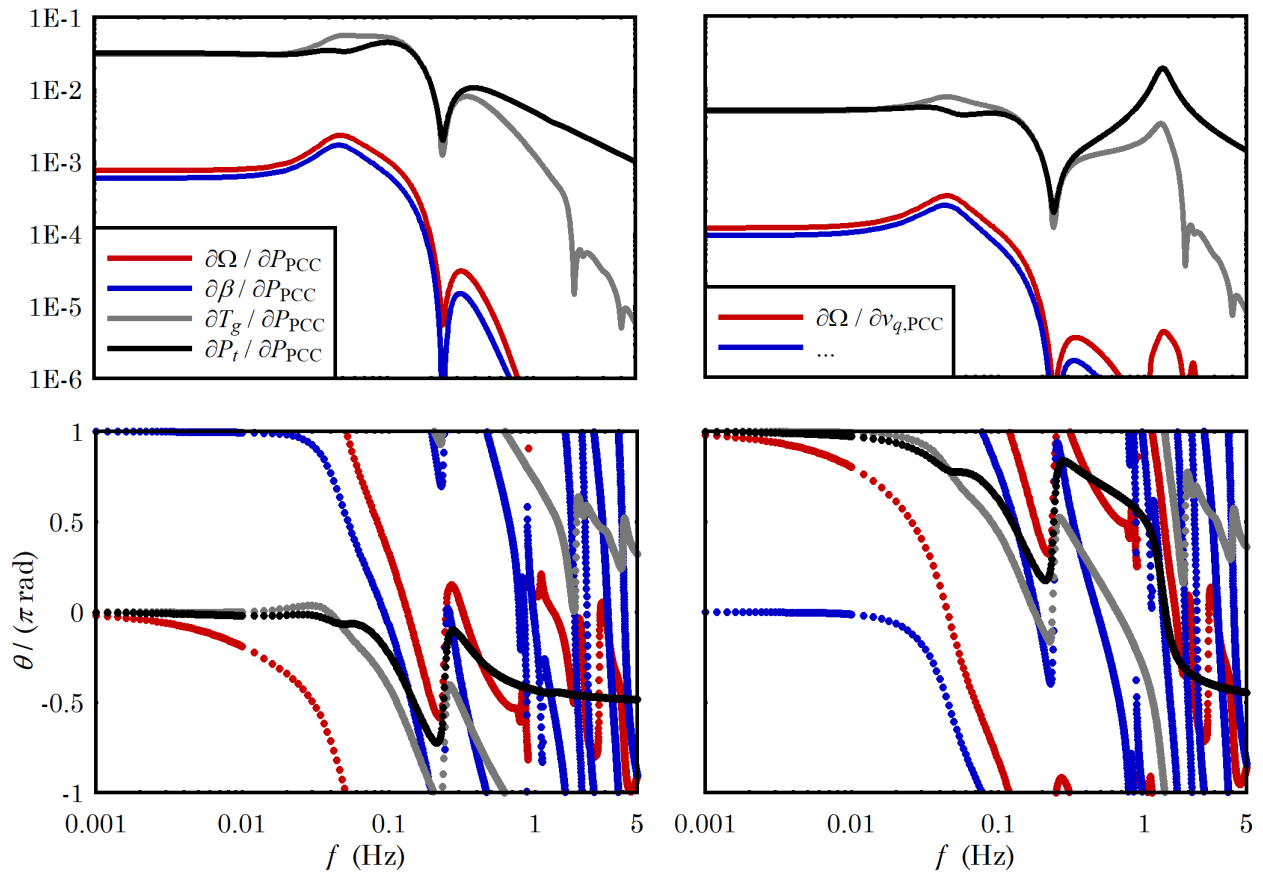
REPORT NUMBER
D4.6

VERSION
1.0

27 of 47

Figure 20: *The response of a wind power plant to perturbations in the PCC power command and q-axis voltage. Units of power are MW, torque MNm, rotor speed rad/s, angles radians, and voltage kV.*
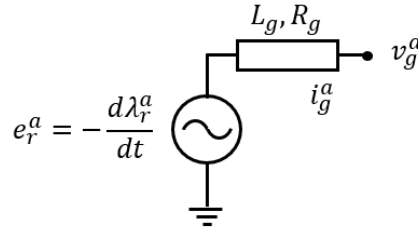
PROJECT
TotalControl

REPORT NUMBER
D4.6

VERSION
1.0

28 of 47

Figure 21: An equivalent circuit diagram of one of the synchronous generator phases, phase 'a'.

3.6 Characterizing the onshore electric grid

The onshore grid is characterized in a realistic way by modelling thermal and hydroelectric power stations in some detail.

3.7 Thermal generation

For a representative thermal plant we adopt a 555 MW fossil-fired steam unit, used extensively by Kundur (1994) in examples on power system stability. The relevant components include a long drive-shaft with concentrated masses representing various turbine stages, and a synchronous generator with static excitation.

The generator electric circuit is modelled as a controllable voltage source feeding through an impedance, Fig. 21 showing an example of one of the three phases. The generator has a physical rotor that rotates inside a set of stator windings. We can easily measure and understand the angle of the magnetic North pole of the rotor relative to the stator a phase; let this angle be θ_g. The strength of the rotor flux linking the stator a winding is

$$\lambda_r^a = \overline{\lambda}_r \cos \theta_g, \tag{8}$$

where $\overline{\lambda}_r$ is the magnitude of the flux, which can be controlled by modulating the rotor field strength.

The electrical state equation for a single phase is

$$L_g \frac{di_g^a}{dt} = -R_g i_g^a - v_g^a - \frac{d\lambda_r^a}{dt}. \tag{9}$$

Here mutual inductances between stator phases are ignored, as are other secondary electromagnetic effects that would make the equivalent circuit of Fig. 21 more complicated. Stacking the equations for the three phases and applying the power-equivalent d-q transformation,

$$\mathbf{T}_a^\theta = \sqrt{\frac{2}{3}} \begin{bmatrix} \cos\theta & \cos(\theta - 2\pi/3) & \cos(\theta - 4\pi/3) \\ -\sin\theta & -\sin(\theta - 2\pi/3) & -\sin(\theta - 4\pi/3) \end{bmatrix}, \tag{10}$$

with inverse

$$\mathbf{T}_\theta^a = \sqrt{\frac{2}{3}} \begin{bmatrix} \cos\theta & -\sin\theta \\ \cos(\theta - 2\pi/3) & -\sin(\theta - 2\pi/3) \\ \cos(\theta - 4\pi/3) & -\sin(\theta - 4\pi/3) \end{bmatrix}, \tag{11}$$

gives

$$\mathbf{T}_a^\theta \mathbf{L}_g \mathbf{T}_\theta^a \frac{d\mathbf{i}_g^\theta}{dt} = -\left(\omega_g \mathbf{T}_a^\theta \mathbf{L}_g \frac{d\mathbf{T}_\theta^a}{d\theta^a} + \mathbf{T}_a^\theta \mathbf{R}_g \mathbf{T}_\theta^a \right) \mathbf{i}_g^\theta - \mathbf{v}_g^\theta - \omega_g \mathbf{T}_a^\theta \frac{d\mathbf{T}_\theta^a}{d\theta} \boldsymbol{\lambda}_r^\theta. \tag{12}$$

Here the vectors should be interpreted as follows. Taking the voltage as an example, define the instantaneous phase a voltage as

$$v_g^a = \overline{v}_g \cos \theta_v, \tag{13}$$

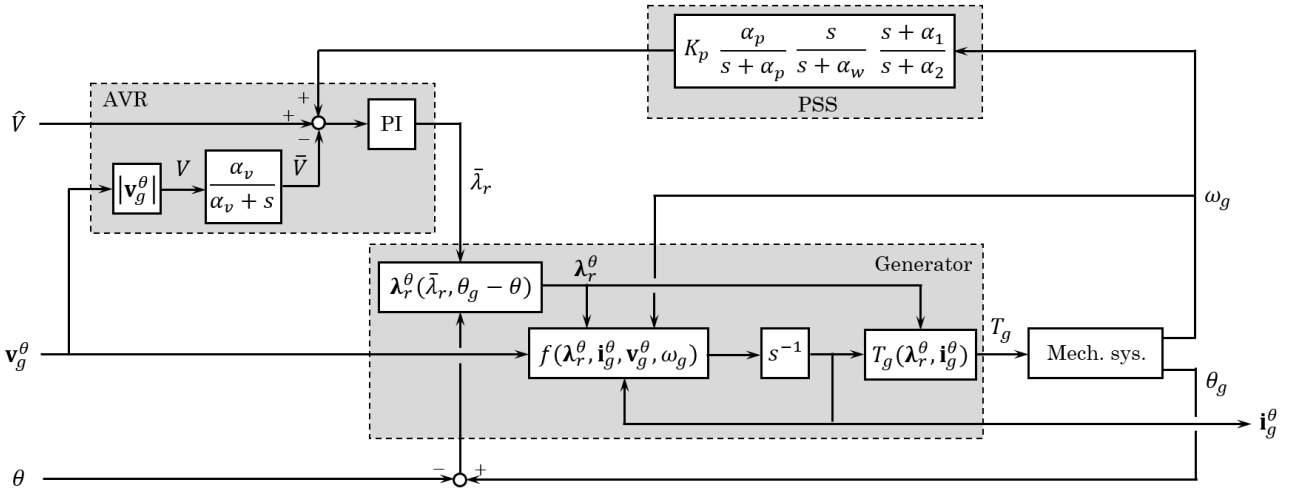PROJECT
TotalControl

REPORT NUMBER
D4.6

VERSION
1.0

29 of 47

Figure 22: A block diagram of a synchronous generator with automatic voltage regulation (AVR) and power-system stabilization (PSS).

where $\overline{v}_g$ is the amplitude. Then

$$\mathbf{v}_g^\theta = \mathbf{T}_a^\theta \overline{v}_g \begin{bmatrix} \cos\theta_v \\ \cos(\theta_v - 2\pi/3) \\ \cos(\theta_v - 4\pi/3) \end{bmatrix} = \sqrt{\frac{3}{2}} \overline{v}_g \begin{bmatrix} \cos(\theta_v - \theta) \\ \sin(\theta_v - \theta) \end{bmatrix} := \begin{bmatrix} v_{g,d}^\theta \\ v_{g,q}^\theta \end{bmatrix}. \tag{14}$$

Note that when the grid is operating at a steady state, since θ_v and θ are rotating at the same frequency, the values of $\mathbf{v}_g^\theta$ will be steady; the AC frequency has been factored out of the state equations. A change in the AC frequency of the generator relative to the grid reference will be seen as a steady drift of the d and q components of $\mathbf{v}_g^\theta$. A similar statement can be made for the current $\mathbf{i}_g^\theta$ and flux $\boldsymbol{\lambda}_r^\theta$. The air-gap torque is

$$T_g = -\frac{1}{2} n_p \mathbf{T}_a^\theta \frac{d\mathbf{T}_\theta^a}{d\theta} \boldsymbol{\lambda}_r^\theta \cdot \mathbf{i}_g^\theta, \tag{15}$$

where

$$\mathbf{T}_a^\theta \frac{d\mathbf{T}_\theta^a}{d\theta^a} = \begin{bmatrix} 0 & -1 \\ 1 & 0 \end{bmatrix}. \tag{16}$$

If we are willing to accept some simplification of the generator model behind (12), namely omitting mutual inductances such that $\mathbf{R}_g$ and $\mathbf{L}_g$ are diagonal matrices, then the equation can be simplified to

$$L_g \frac{d\mathbf{i}_g^\theta}{dt} = -\left(\omega_g L_g \begin{bmatrix} 0 & -1 \\ 1 & 0 \end{bmatrix} + R_g \mathbf{I}\right) \mathbf{i}_g^\theta - \mathbf{v}_g^\theta - \omega_g \begin{bmatrix} 0 & -1 \\ 1 & 0 \end{bmatrix} \boldsymbol{\lambda}_r^\theta, \tag{17}$$

where L_g and R_g are the phase inductance and resistance from (9).

The synchronous generator is equipped with a set of controls that govern the exciter current, and hence the strength of the flux $\overline{\lambda}_r$. For the present purposes, the particulars of the rotor windings do not need to be considered, and we can consider $\overline{\lambda}_r$ to be directly controllable. There are two control functions, as shown in Fig. 22: automatic voltage regulation (AVR) and power-system stabilization (PSS). This model is adapted from Section 12.5 of Kundur (1994).

The generator rotor is connected to a shaft, which in turn is connected to a series of four steam turbines: one high-pressure, one intermediate-pressure, and two low-pressure stages. Each steam turbine has a rotational inertia, and each shaft segment between turbines has an elastic torsional stiffness and damping. The equations describing the mechanical system are

$$\begin{bmatrix} \mathbf{I} & \mathbf{0} \\ \mathbf{0} & \mathbf{J} \end{bmatrix} \frac{d}{dt} \begin{bmatrix} \delta\boldsymbol{\Theta} \\ \boldsymbol{\Omega} \end{bmatrix} = \begin{bmatrix} \mathbf{0} & \mathbf{I} \\ -\mathbf{K} & -\mathbf{C} \end{bmatrix} \begin{bmatrix} \delta\boldsymbol{\Theta} \\ \boldsymbol{\Omega} \end{bmatrix} + \begin{bmatrix} -1 & \mathbf{0} \\ \mathbf{0} & \mathbf{I} \end{bmatrix} \begin{bmatrix} \Omega_e \\ \mathbf{T} \end{bmatrix} \tag{18}$$

PROJECT
TotalControl

REPORT NUMBER
D4.6

VERSION
1.0

30 of 47

with

$$
\delta\boldsymbol{\Theta} = \begin{bmatrix} \Theta_H \\ \Theta_I \\ \Theta_1 \\ \Theta_2 \\ \Theta_g \end{bmatrix} - \Theta_e, \qquad \boldsymbol{\Omega} = \begin{bmatrix} \Omega_H \\ \Omega_I \\ \Omega_1 \\ \Omega_2 \\ \Omega_g \end{bmatrix} \tag{19}
$$

$$
\mathbf{J} = \begin{bmatrix} J_H & & & & \\ & J_I & & 0 & \\ & & J_1 & & \\ & 0 & & J_2 & \\ & & & & J_g \end{bmatrix} \tag{20}
$$

$$
\mathbf{K} = \begin{bmatrix} k_H & -k_H & 0 & 0 & 0 \\ -k_H & k_H + k_I & -k_I & 0 & 0 \\ 0 & -k_I & k_I + k_1 & -k_1 & 0 \\ 0 & 0 & -k_1 & k_1 + k_2 & -k_2 \\ 0 & 0 & 0 & -k_2 & k_2 \end{bmatrix} \tag{21}
$$

$$
\mathbf{C} = \begin{bmatrix} c_H & -c_H & 0 & 0 & 0 \\ -c_H & c_H + c_I & -c_I & 0 & 0 \\ 0 & -c_I & c_I + c_1 & -c_1 & 0 \\ 0 & 0 & -c_1 & c_1 + c_2 & -c_2 \\ 0 & 0 & 0 & -c_2 & c_2 \end{bmatrix} \tag{22}
$$

$$
\mathbf{T} = \begin{bmatrix} T_H \\ T_I \\ T_1 \\ T_2 \\ -T_g \end{bmatrix} \tag{23}
$$

Here Θ_g is the mechanical angle of the generator rotor, related to θ_g by

$$
\Theta_g = \frac{2}{n_p} \theta_g, \tag{24}
$$

n_p being the number of poles. The same relationship applies between Ω_g and ω_g, Θ_e and θ_e, and Ω_e and ω_e. We might take the damping to be proportional to the stiffness, in which case $\mathbf{C} = \kappa\mathbf{K}$ with κ a tunable parameter. As a rule-of-thumb κ should be tuned such that the structural damping ratio of the lower-frequency mechanical oscillations is in the vicinity of $\zeta = 0.005$.

The steam turbine torque is regulated by actuator valves that throttle the flow of steam. The response of the steam turbines to the throttle may be represented by a simple set of transfer functions (Kunder 1994, p 426)

$$
T_H = \frac{\alpha_C}{s + \alpha_C} \beta_H \tau \tag{25}
$$

$$
T_I = G(s)\,\beta_I \tau, \quad T_1 = G(s)\,\beta_1 \tau, \quad T_2 = G(s)\,\beta_2 \tau \tag{26}
$$

with

$$
G(s) = \frac{\alpha_C}{s + \alpha_C} \frac{\alpha_R}{s + \alpha_R} \tag{27}
$$

The β parameters represent the fraction of torque delivered by each turbine stage, which is assumed to be constant, and must sum to unity. Also, τ is the torque control signal sent to the valve, and α_C and α_R are time constants representing the flow of steam through piping and other components.

PROJECT
TotalControl

REPORT NUMBER
D4.6

VERSION
1.0

31 of 47

Table V: Default values of the parameters describing a 555 MVA thermal power station.

J_H	1395	kg m^2	Inertia of high-pressure turbine
J_I	2609	kg m^2	Inertia of intermediate-pressure turbine
J_1	12990	kg m^2	Inertia of low-pressure turbine 1
J_2	13406	kg m^2	Inertia of low-pressure turbine 2
J_g	9616	kg m^2	Inertia of generator rotor
K_H	3.851×10^7	N m/rad	Stiffness of HP-IP shaft
K_I	8.550×10^7	N m/rad	Stiffness of IP-LP1 shaft
K_1	1.336×10^8	N m/rad	Stiffness of LP1-LP2 shaft
K_2	1.101×10^8	N m/rad	Stiffness of LP2-generator shaft
κ	0.0001	s	Stiffness-proportional damping parameter
n_p	2	-	Number of generator poles
L_g	0.0075	H	Generator stator winding inductance
R_g	0.0031	Ω	Generator stator winding resistance
α_v	0.2	Hz	AVR LP filter frequency
K_{Pv}	0.02	Wb/V	AVR proportional gain
K_{Iv}	0.002	Wb/Vs	AVR integral gain
α_L	5.0	Hz	PSS LP filter frequency
α_w	0.1	Hz	PSS HP (washout) filter frequency
α_1	8.0	Hz	PSS phase-shift numerator
α_2	4.0	Hz	PSS phase-shift denominator
K_{PSS}	100.0	Vs	PSS gain
K_P	0.07	s/rad	Grid frequency droop gain
K_I	0.0	1/rad	Grid frequency integral gain
α_C	3.3	Hz	Steam chest time constant
α_R	0.17	Hz	Reheat time constant
α_s	1.0	Hz	Servo-control time constant
β_H	0.3	-	Fraction of torque from HP turbine
β_I	0.3	-	Fraction of torque from IP turbine
β_1	0.2	-	Fraction of torque from LP1 turbine
β_2	0.2	-	Fraction of torque from LP2 turbine

The thermal plant is equipped with a primary speed controller, implementing droop control on the frequency deviation measured at the generator. This takes the form

$$\tau = \frac{\alpha_\omega}{s + \alpha_\omega} \left[1 - K_P \varepsilon_\omega - \Psi_\omega\right] \hat{T}_g \tag{28}$$

with

$$\varepsilon_\omega = \overline{\omega}_g - \hat{\omega}_g \tag{29}$$

the frequency error and

$$\Psi_\omega = \int_0^t K_I \varepsilon_\omega \, dt = K_I \frac{\varepsilon_\omega}{s}. \tag{30}$$

the integrated error. Also, $\hat{T}_g$ and $\hat{\omega}_g$ are torque and speed references, $\overline{\omega}_g$ is the measured shaft speed, K_P and K_I are the proportional and integral gains, and α_ω represents the rate of the speed controller.

Values of parameters describing the thermal power station are listed in Table V.

Figure 23 illustrates the low-frequency response of the thermal power plant to perturbations in the power command, grid frequency, and grid voltage. The shaft torsional resonant frequencies are in the range of 14 Hz and above, and do not appear in the plots. There is one prominent resonant mode at around 1 Hz, associated with resonance of the synchronous generator about the electromagnetic restoring torque of the field and windings. The upper-left plot indicates that the plant can accurately track a power command up to a frequency of about 0.2 Hz. The upper-right plot shows the response

PROJECT
TotalControl

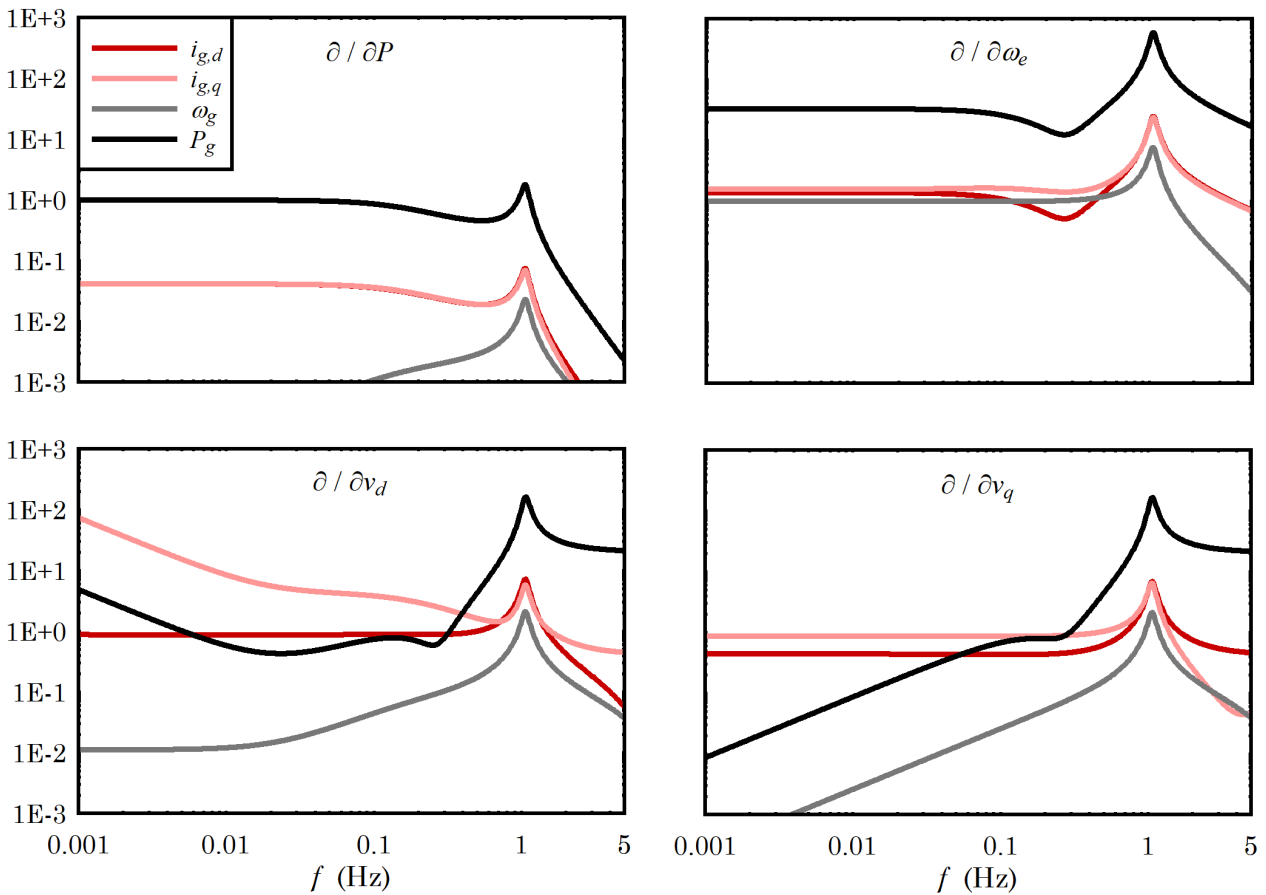REPORT NUMBER
D4.6

VERSION
1.0

32 of 47

Figure 23: Transfer functions illustrating the input-output response of the thermal power station. Units of power are MW, generator and electrical speeds rad/s, currents kA, and voltages kV.

of the frequency droop control; the integral gain is set to zero as a default. The AVR control of the exciter is visible in the plot at lower-left, including slow integral action over a period of a minute or more.

In the analyses of Section 3.9, the thermal power station is generating 500 MW as an initial steady-state operating condition.

3.8 Hydroelectric generation

Figure 24 shows the waterway of a hydroelectric power plant. In this idealized model there is a single tunnel from the primary water source; a penstock at a steep slope feeding into the power station; an open-air surge shaft at the top of the penstock; and, in the power station, a Francis turbine with draft tube. The flow physics including compressibility (resonance) effects are modelled using a finite-difference technique, and a semi-empirical model based on the Euler equation describes the dynamics of the Francis turbine and draft tube (Merz 2019c). The node numbering scheme is indicated in the figure,[7] along with length and height dimensions.

Let us first consider the waterway, not including the turbine and draft tube. The flow at each node is described by a pressure variable q_1,

$$q_1 = \sqrt{\kappa} A p, \tag{31}$$

---

[7]The number of nodes is reduced for convenient sketching; for a given geometry, a convergence study should be performed to make sure that there is a sufficient number of nodes.

PROJECT
TotalControl

REPORT NUMBER
D4.6

VERSION
1.0

33 of 47
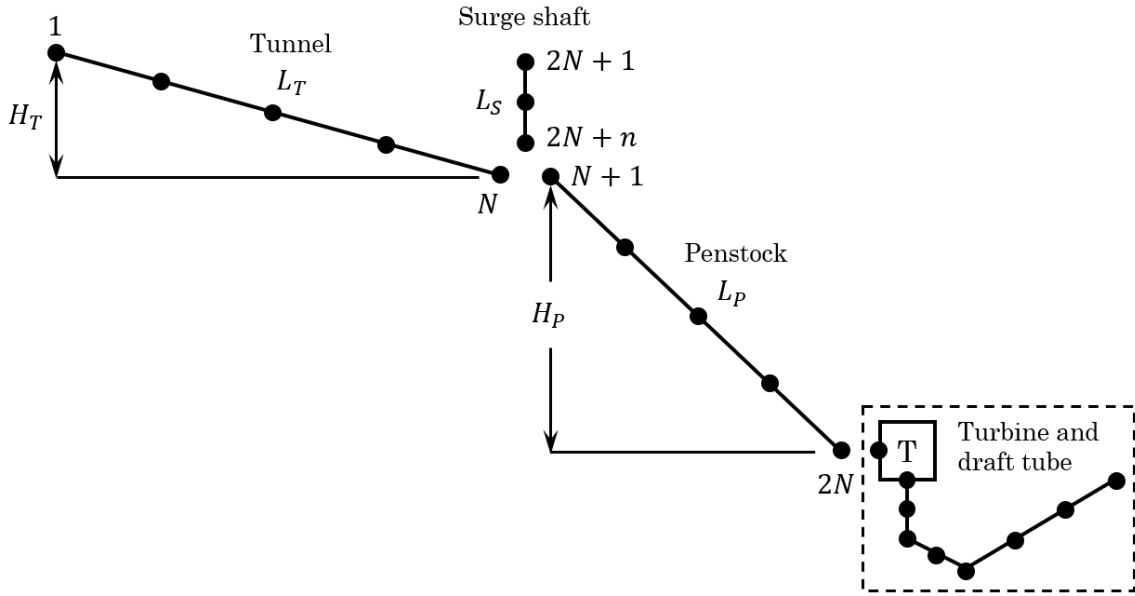
Figure 24: A sketch of the hydroelectric power plant waterway model.

where κ is a compressibility parameter such that

$$\rho = \rho_0 + \kappa p, \tag{32}$$

A is the cross-sectional area, and p is the fluid pressure; and a flow-rate variable q_2,

$$q_2 = \rho A v, \tag{33}$$

where v is the bulk fluid velocity. The nodal variables may be stacked into a common vector $\mathbf{q}$. At each boundary node in the waterway network, either the pressure (via q_1) or the flow rate (via q_2) must be prescribed. In the model of Fig. 24, the pressure is prescribed at Nodes 1 (tunnel inlet) and $2N + 1$ (shaft inlet), and the flow rate is prescribed at Node $2N$ (penstock outlet). In addition, there are conditions at the intersection of Nodes N, $N + 1$, and $2N + n$; namely, the pressure at these three nodes must be identical,[8]

$$\frac{q_1^N}{A^N} = \frac{q_1^{N+1}}{A^{N+1}} = \frac{q_1^{2N+n}}{A^{2N+n}}, \tag{34}$$

and mass balance must be satisfied via

$$q_2^N + q_2^{2N+n} = q_2^{N+1}. \tag{35}$$

The constraints can be written in the form

$$\mathbf{Lq} = \mathbf{0}. \tag{36}$$

We can partition (36) into retained and slave degrees-of-freedom,

$$\mathbf{L}_s \mathbf{q}_s + \hat{\mathbf{L}}\hat{\mathbf{q}} = \mathbf{0}, \tag{37}$$

and define a matrix

$$\mathbf{\Lambda} = \begin{bmatrix} \mathbf{I} \\ -\mathbf{L}_s^{-1}\hat{\mathbf{L}} \end{bmatrix} \tag{38}$$

---

[8]The $\sqrt{\kappa}$ factors cancel.

PROJECT
TotalControl

REPORT NUMBER
D4.6

VERSION
1.0

34 of 47

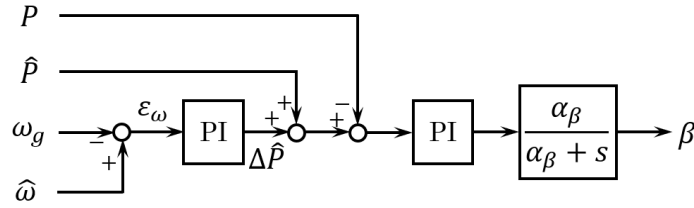*Figure 25: The gate control algorithm including grid frequency droop.*

that relates the reduced vector to the full vector of variables, as[9]

$$\mathbf{q} = \mathbf{\Lambda}\hat{\mathbf{q}}, \qquad \frac{d\mathbf{q}}{dt} = \mathbf{\Lambda}\frac{d\hat{\mathbf{q}}}{dt}. \tag{39}$$

Writing the unconstrained pipe equations gives

$$\frac{d\mathbf{q}}{dt} = \mathbf{f}(\mathbf{q}, \mathbf{u}) = \mathbf{f}(\mathbf{\Lambda}\hat{\mathbf{q}}, \mathbf{u}), \tag{40}$$

which can be solved approximately using a generalized inverse,

$$\frac{d\hat{\mathbf{q}}}{dt} = \left(\mathbf{\Lambda}^T\mathbf{\Lambda}\right)^{-1}\mathbf{\Lambda}^T\mathbf{f}(\mathbf{\Lambda}\hat{\mathbf{q}}, \mathbf{u}), \tag{41}$$

with the linearized equations

$$\frac{d\Delta\mathbf{q}}{dt} = \left(\mathbf{\Lambda}^T\mathbf{\Lambda}\right)^{-1}\left(\mathbf{\Lambda}^T\mathbf{A}\mathbf{\Lambda}\,\Delta\hat{\mathbf{q}} + \mathbf{\Lambda}^T\mathbf{B}\,\Delta\mathbf{u}\right). \tag{42}$$

The turbine and draft tube connect to the penstock outlet node of the waterway model. At this node, the turbine owns the flow rate q_2, and the waterway node owns the pressure variable q_1. The draft tube is modelled using a finite difference technique, just like the waterway, although there are some special features to represent the effects of the turbine's wake. In particular, a representation of a vapor core appears when there is a strong swirl in the wake. This vapor core is highly compressible in comparison with liquid water, and it can influence the natural frequencies of the system.

The turbine is represented as a rotating inertia acted on by two torques, the hydrodynamic torque from the runner and the electrical torque from the generator. The generator in the present case is a 24-pole, 350 MW, synchronous machine. The electrical equations from Section 3.7 apply here as well.

The power of the hydroelectric turbine is set by adjusting the angle of a wicket gate. The gate control algorithm is sketched in Fig. 25. It consists of an inner power controller, adjusting the gate angle β so as to track a commanded power; and an outer frequency-droop controller, which in turn acts through a power command.

The generator is a large-diameter 24-pole synchronous machine. The dynamic equations including AVR controls are the same as for the thermal generator in Section 3.7.

Parameters describing the hydroelectric plant are listed in Tables VI and VII.

Figure 26 shows how the hydroelectric plant responds to power commands and changes in the grid frequency. The left-hand plots show the magnitude and phase of the response of the generator power, runner inlet pressure, gate angle, and rotor speed to an operator power command, which is implemented via the gate controls. Likewise, the right-hand plots show the magnitude and phase of the response to the grid frequency, which directly affects the dynamics of the generator, with slow-acting compensation by frequency droop control.[10]

---

[9]The time derivative takes this simple form since (36) is a linear equation so that $\mathbf{L}$ is constant. In the more general case where the constraints depend nonlinearly on the states, things get more complicated: see for example the treatment of multibody aeroelastic equations in Merz (2018).

[10]The synchronous generator indeed follows the grid frequency, however since there are 24 poles the change in the generator and runner speed is only $1/12^{\text{th}}$ of the change in electrical frequency.

PROJECT
TotalControl

REPORT NUMBER
D4.6

VERSION
1.0

35 of 47

Table VI: Default values of the parameters describing a 350 MW hydroelectric power plant.

N	41	-	Number of nodes, tunnel and penstock
n	3	-	Number of nodes, surge shaft
p_a	1×10^5	Pa	Ambient pressure
κ	4.618×10^{-7}	s^2/m^2	$\rho = \rho_0 + \kappa p$
ρ	1000	kg/m^3	Water density
L_T	4000	m	Tunnel length
H_T	50	m	Tunnel vertical drop
A_T	$\pi(3^2)/4$	m^2	Tunnel cross-sectional area
$C_{f,T}$	0.02	-	Tunnel friction coefficient
L_P	1500	m	Penstock length
H_P	535	m	Penstock vertical drop
A_P	$\pi(2.5^2)/4$	m^2	Penstock cross-sectional area
$C_{f,P}$	0.02	-	Penstock friction coefficient
L_S	40	m	Surge shaft height to terminating node
A_S	$\pi(2^2)/4$	m^2	Surge shaft cross-sectional area
$C_{f,S}$	0.035	-	Surge shaft friction coefficient
φ	2×10^4	-	Numerical damping parameter
ψ_r	19.62	deg	Runner trailing edge angle
γ_r	77.4	deg	Runner leading edge angle
κ_r	1	-	Loss coefficient for incidence/shock
g_f	0.1	-	Loss coefficient for gate opening
$C_{f,r}$	0.015	-	Runner friction coefficient
g	9.81	m/s^2	Gravitational constant
M	10850	kg	Effective fluid mass within the runner
J	8.24×10^5	kg m^2	Effective inertia of the turbine
A_I	7.069	m^2	Volute inlet cross-sectiional area
A_R	8.212	m^2	Runner inlet cross-sectiional area
A_O	6.762	m^2	Volute outlet cross-sectiional area
r_R	2.648	m	Runner inlet radius
r_O	1.037	m	Runner outlet radius
L_r	1.467	m	Effective runner channel length
d_h	0.171	m	Runner channel hydraulic diameter
z_I	0.841	m	Elevation of turbine inlet
z_O	0.168	m	Elevation of turbine outlet
N_{da}	5	-	Number of elements, draft tube cone
N_{db}	7	-	Number of elements, draft tube elbow
N_{dc}	9	-	Number of elements, draft tube diffuser
L_a	3.903	m	Length of draft tube cone
L_b	9.771	m	Length of draft tube elbow
L_c	17.84	m	Length of draft tube diffuser
D_i	0	m	Inner turbine outlet diameter
D_o	2.934	m	Outer turbine outlet diameter
Φ	100	-	Numerical diffusion parameter

PROJECT
TotalControl

REPORT NUMBER
D4.6

VERSION
1.0

36 of 47

Table VII: Default values of generator and control parameters for a 350 MW hydroelectric power plant.

n_p	24	-	Number of generator poles
L_g	0.0105	H	Generator stator winding inductance
R_g	0.0043	Ω	Generator stator winding resistance
α_v	0.2	Hz	AVR LP filter frequency
K_{Pv}	0.02	Wb/V	AVR proportional gain
K_{Iv}	0.002	Wb/Vs	AVR integral gain
α_L	5.0	Hz	PSS LP filter frequency
α_w	0.1	Hz	PSS HP (washout) filter frequency
α_1	8.0	Hz	PSS phase-shift numerator
α_2	4.0	Hz	PSS phase-shift denominator
K_{PSS}	100.0	Vs	PSS gain
α_L	0.1	Hz	LP filter frequency
$K_{P\omega}$	2.4×10^7	Ws/rad	Grid frequency droop gain
$K_{I\omega}$	0.0	W/rad	Grid frequency integral gain
K_P	2.5×10^{-10}	rad/W	Gate angle power control gain
K_I	2.5×10^{-11}	rad/Ws	Gate angle power control integral gain

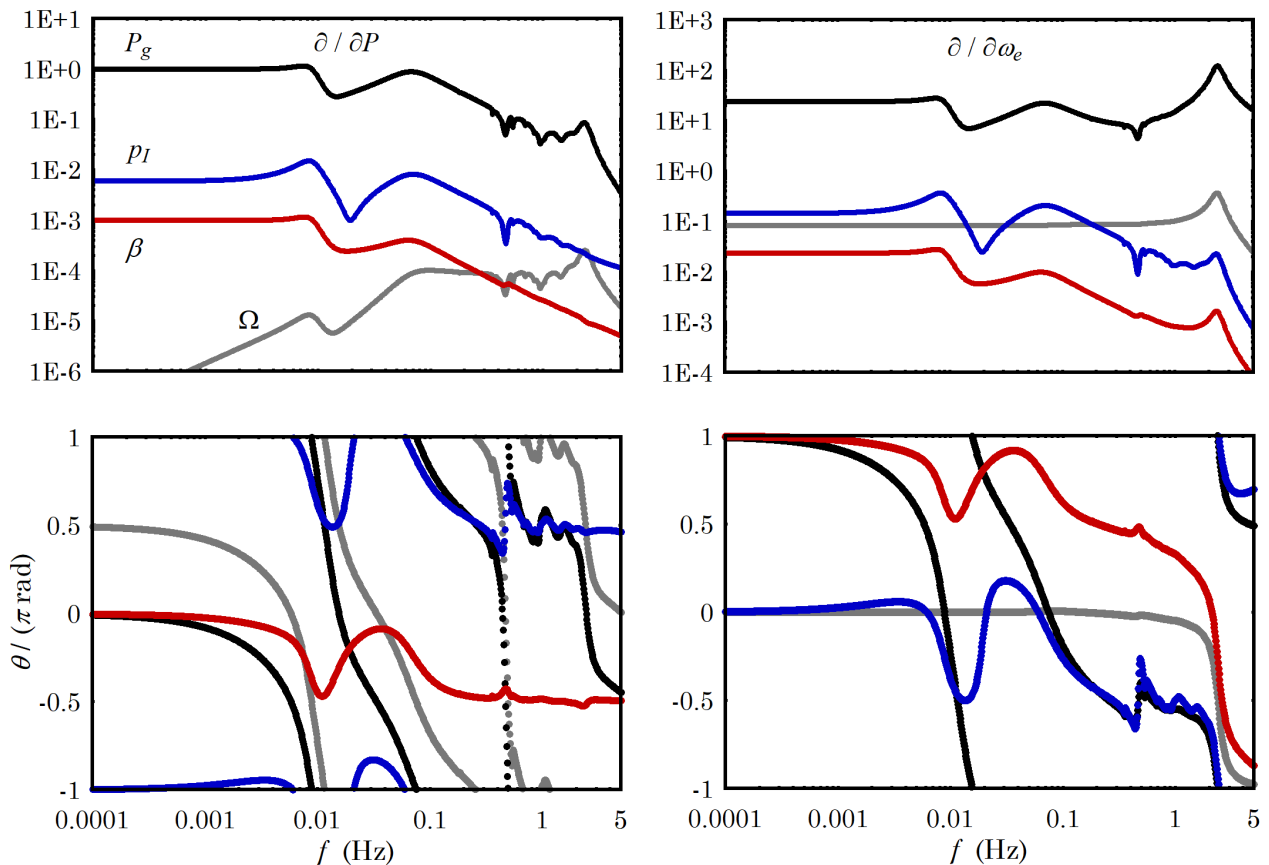*Figure 26: Transfer functions showing the response of the hydroelectric power station to power command and grid frequency inputs. Here P_g is generator power, p_I the pressure at the runner inlet, β the gate angle, and Ω the runner rotational speed. Units of power are MW, pressure MPa, runner and electrical speeds rad/s, and angles radians.*

PROJECT
TotalControl

REPORT NUMBER
D4.6

VERSION
1.0

37 of 47

The hydroelectric plant is more active dynamically than was the thermal plant of Section 3.7. The prominant feature of the hydroelectric plant's dynamic response is a non-minimum phase zero at around 0.01 Hz. This is associated with flow into and out of the surge shaft as it accommodates pressure changes in the tunnel, with some delay. There are also myriad hydraulic resonant modes above 0.1 Hz, although these do not appear strongly in the system response to the selected inputs. Finally, there is a prominant resonant mode at 2.4 Hz associated with the electromagnetic restoring torque of the synchronous generator.

In the analyses that follow, the hydroelectric plant is generating its rated power of 350 MW as an initial steady-state operating condition.

3.9   Electric grid connection and control scenarios

Three scenarios are considered: a wind plant connected to a strong grid, with focus on the collection and transmission systems associated with the plant; a scenario in which a wind plant, thermal plant, and hydroelectric plant are connected at a common onshore bus, feeding through a transmission line to a strong grid (voltage source); and a scenario with the same three generation sources, supplying an isolated electrical load.

3.10   Wind plant on a strong grid

A strong grid does not respond to changes in the power generated by the wind plant. In the limit, a strong grid can be modelled by prescribing the voltage and frequency at the onshore PCC, making these independent of the current injected by the wind plant.

Even though the wind plant is connected to a strong onshore grid, this does not mean that the plant's collection and transmission grid is strong. The voltage seen by a given wind turbine's MV transformer terminals will be a function of the current injected by *all* of the turbines. This sensitivity tends to destabilize the active and reactive power control of the turbine's network-side converter, in comparison with the infinite-bus case, resulting in a plantwide oscillatory mode. In the present case of the TotalControl Reference Wind Power Plant, the mode has a frequency around 1.3 Hz and a damping ratio of about 0.13. When the wind plant's PCC power is measured and fed back to the wind turbines, by way of the dispatch control function, this mode appears in the generator torque (Fig. 20), and hence is transmitted (albeit weakly) to the mechanical system.

The current-control mode under consideration differs from the well-known resonant mode of a synchronous generator feeding an impedance (Kundur 1994). The wind turbines' generators are effectively isolated from the grid by the converters and DC link. Here the resonant mode is related to the tuning of the DC link voltage control and reactive power control provided by the network-side converter.

The current-control mode consists of a nearly equal response from all the wind turbines. It can therefore be accurately reproduced with a lumped model, retaining only one turbine's dynamic states and injecting an identical, synchronized current into the collection grid at each turbine's bus. Table VIII summarizes the characteristics of the mode shape, normalized to the *d*-axis voltage fluctuation at the turbine transformer terminals. The mode shape hints how oscillations are set up between the *d*-axis control of the DC link voltage (active power) and the *q*-axis control of reactive power, interacting with the terminal voltages.

The current-control mode exists due to mistuning of the vector control law of the network side converter. This control law employs a type of feedback linearization – a nonlinear model-based correction to the control law – to obtain a favorable control dynamic (Merz 2019b, Anaya-Lara 2009). An effective inductance must be provided as part of the nonlinear model embedded in the controller. This inductance was originally set to be that of the wind turbine's MV transformer, assuming that the turbine would be connected to a strong grid. However, the effective inductance of the Reference Wind Plant, with its transmission to shore, is an order of magnitude greater. The effective inductance

Table VIII: The mode shape of selected variables participating in the current-control mode ($f = 1.3$ Hz, $\zeta = 0.13$).

Variable	$|\varphi|$	$\theta/(\pi\,\mathrm{rad})$	Description
	No plant control		
$i^{\theta}_{\mathrm{PCC},d}$	4.9×10^{-2}	-0.471	PCC d-axis current, kA
$i^{\theta}_{\mathrm{PCC},q}$	8.8×10^{-2}	-0.971	PCC q-axis current, kA
$i^{\theta}_{s,d}$	9.2×10^{-3}	-0.470	Turbine d-axis current, kA
$i^{\theta}_{s,q}$	1.6×10^{-2}	-0.970	Turbine q-axis current, kA
$v^{\theta}_{s,d}$	1.0×10^{0}	0.000	Turbine d-axis voltage, kV
$v^{\theta}_{s,q}$	5.6×10^{-1}	-0.519	Turbine q-axis voltage, kV
V_{DC}	2.7×10^{0}	0.077	Turbine DC link voltage, kV
$\widehat{P}_t$	0	-	Dispatch power command, MW
T_g	0	-	Turbine generator torque, MNm
Ω	0	-	Turbine rotor speed, rad/s
	With plant control		
$i^{\theta}_{\mathrm{PCC},d}$	4.9×10^{-2}	-0.473	PCC d-axis current, kA
$i^{\theta}_{\mathrm{PCC},q}$	8.8×10^{-2}	-0.971	PCC q-axis current, kA
$i^{\theta}_{s,d}$	9.1×10^{-3}	-0.471	Turbine d-axis current, kA
$i^{\theta}_{s,q}$	1.6×10^{-2}	-0.970	Turbine q-axis current, kA
$v^{\theta}_{s,d}$	1.0×10^{0}	0.000	Turbine d-axis voltage, kV
$v^{\theta}_{s,q}$	5.6×10^{-1}	-0.520	Turbine q-axis voltage, kV
V_{DC}	2.7×10^{0}	0.077	Turbine DC link voltage, kV
$\widehat{P}_t$	3.8×10^{-2}	0.032	Dispatch power command, MW
T_g	8.6×10^{-3}	0.987	Turbine generator torque, MNm
Ω	1.1×10^{-5}	0.614	Turbine rotor speed, rad/s

can be estimated by perturbing the current from the wind turbine and observing the change in the terminal voltage:

$$L = \omega_e^{-1} \frac{\Delta v^{\theta}_{s,q}}{\Delta i^{\theta}_{s,d}} \tag{43}$$

Once this was recalibrated to the true value, the current-control mode disappeared, giving the revised transfer functions shown as dashed lines in Fig. 27. The retuned wind turbine model is used in all the subsequent analyses.

It is concluded that the vector control law of the network side converter must be tuned according to the in-situ effective impedance, which may vary significantly from location to location. The modal dynamics of the network-side current control must account for the fact that all turbines may respond synchronously to a perturbation in grid voltage or an operator power command. Unfavorable current-control dynamics may affect the structural response of the wind turbine via the plant dispatch controller, although the structural response has very little influence back on the current-control dynamics. Additional filters might be introduced to the plant controller in order to prevent the possibility of interaction in the event that the effective grid inductance changes unexpectedly, for instance with the loss of a transmission line.

3.11 Interaction between multiple power plants operating as part of a strong grid

Consider a scenario where an offshore wind power plant, thermal power plant, and hydroelectric power plant are connected to a common bus, with a 132 kV transmission line to a strong grid (voltage source). The grid sets the electrical frequency, which for modelling purposes is considered to be an external input. The voltage v^{θ}_c at the PCC of the three power plants is a function of the effective impedance

PROJECT
TotalControl

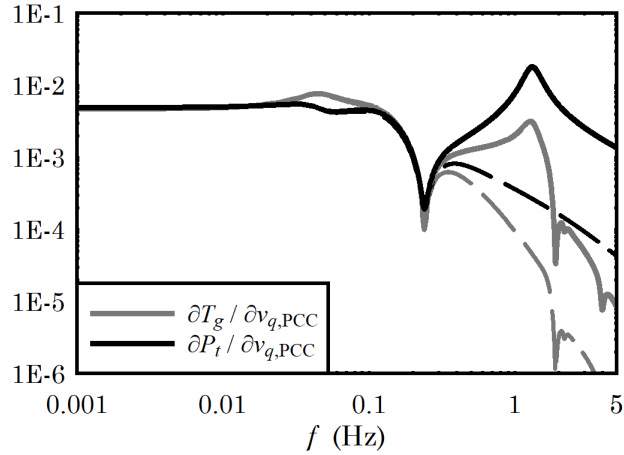REPORT NUMBER
D4.6

VERSION
1.0

39 of 47

Figure 27: Revised transfer functions (dashed lines) after retuning the effective inductance; see Fig. 20.

Table IX: Parameters defining the connection to a strong grid.

$v_{c,d}^{\theta}$	132	kV
$v_{c,q}^{\theta}$	0	kV
i_w^{θ}	$(1442, 0)$	A
i_s^{θ}	$(3775, -1929)$	A
i_h^{θ}	$(2652, -1422)$	A
R	0.302	Ω
L	0.0072	H
C	3.5×10^{-5}	F

to the voltage source,

$$v_c^{\theta} = \left(\omega_e C X \begin{bmatrix} 0 & -1 \\ 1 & 0 \end{bmatrix} + I \right)^{-1} \left(X i_w^{\theta} + X i_s^{\theta} + X i_h^{\theta} + v_0^{\theta} \right), \tag{44}$$

where

$$X = \omega_e L \begin{bmatrix} 0 & -1 \\ 1 & 0 \end{bmatrix} + RI; \tag{45}$$

i_w^{θ}, i_s^{θ}, and i_h^{θ} are the currents injected by respectively the wind, thermal (steam), and hydroelectric generation; and v_0^{θ} is the grid voltage.

Let the resistance, inductance, and capacitance between the PCC and voltage source have the values shown in Table IX. These values are estimated based on transmission cable properties from Merz *et al.* (2019), assuming 60 km distance and 3 parallel cables. Table IX also lists the steady-state PCC voltage and generated currents. Note how the wind plant with its full power conversion provides full control over the reactive power, whereas the synchronous generators' currents lag the voltage.

Figure 28 illustrates the system dynamics of the three power plants feeding a strong grid. The left-hand column of figures shows the generator speeds, wind turbine nacelle displacements, and hydro-electric gate angle. The right-hand column of figures shows the electrical power injected to the PCC from each generation source, "w" for wind, "s" for thermal (steam turbine), and "h" for hydroelectric. The first three rows of figures show the response to power commands, and the final row a change in the grid frequency.

The transfer functions show that there are interactions between a wind plant and other sources of generation, when these are connected at a common bus. The interactions with the wind turbine

PROJECT
TotalControl

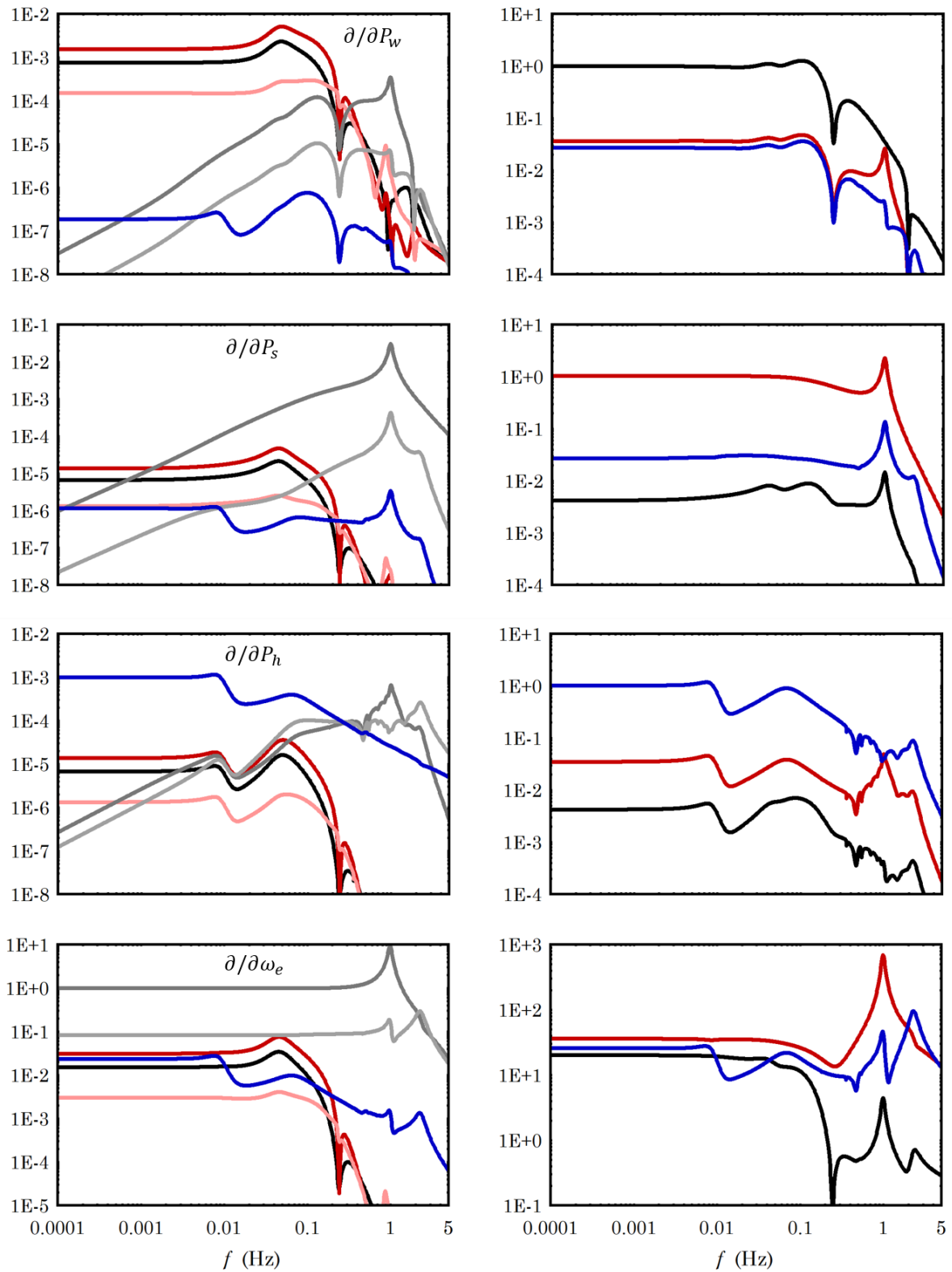REPORT NUMBER
D4.6

VERSION
1.0

40 of 47

Figure 28: Transfer functions illustrating the dynamics of a wind power plant, thermal power plant, and hydroelectric power plant connected to a relatively strong grid. The legend is shown in Fig. 29.

PROJECT
TotalControl

REPORT NUMBER
D4.6

VERSION
1.0

41 of 47

Figure 29: The legend for Fig. 28. The left-hand column of the legend is applicable to the left-hand column of figures, and similarly for the right-hand columns.

Table X: Parameters defining the connection to an isolated grid.

$v_{c,d}^{\theta}$	132	kV
$v_{c,q}^{\theta}$	0	kV
i_w^{θ}	$(1442, 0)$	A
i_s^{θ}	$(3775, -1929)$	A
i_h^{θ}	$(2652, -480)$	A
i_d^{θ}	$i_{w,d}^{\theta} + i_{s,d}^{\theta} + i_{h,d}^{\theta}$	
$i_q^{\theta}/i_d^{\theta}$	-0.5	
R	13.4	Ω
L	0.021	H
C	1.4×10^{-5}	F

structures, seen in the nacelle displacement and rotor speed signals, originate from the wind plant's dispatch controller, and the way in which it reacts to the measured electrical current and voltage at the PCC. The wind plant's response is weak when it comes to changes in the thermal or hydroelectric generation, but the response of the grid frequency droop control is strong, by design.

Not surprisingly, it appears that undesired interactions between interconnected generation sources are mild when the grid is strong. However, interactions do exist: in particular, the AVR control function causes the thermal and hydroelectric plants to respond with a magnitude of a few percent of the change in the wind plant generation (Fig. 28 at upper right). That said, the greatest potential for interaction lies in the grid frequency control, which is required for weak or isolated grids.

3.12 Interaction between multiple power plants operating in isolated system

Consider now the same trio of generation units from Section 3.11, but let them now operate in an isolated system, supplying a load with the properties listed in Table X. There are a variety of ways to model a load (Kundur 1994), but for the present purposes we will consider an impedance that is constant with frequency and voltage. We will, however, perturb the impedance to simulate the connection of an additional load to (or disconnection from) the system. Specifically, we introduce a perturbation factor η such that

$$R = R_0(1 + \eta) \quad \text{and} \quad L = L_0(1 + \eta).$$

The grid frequency can vary. The generator speed of the largest unit, the steam turbine, is taken as the reference for the grid frequency: $\omega_e = \Omega_s$.

We focus on the load perturbation η as an input: someone flips a light switch, plugs in their cell phone, or starts up an aluminum smelter. Figure 30 shows the response. With the default tuning, the dynamics are unfavorable, with prominent resonant modes at 0.009 Hz, with a damping ratio $\zeta = 0.109$, and 0.088 Hz/0.094. The characteristics of these modes are summarized in Table XI. The

PROJECT
TotalControl

REPORT NUMBER
D4.6

VERSION
1.0

42 of 47

Table XI: Characteristics of the resonant modes excited by a change in the grid load.

Variable	0.009 Hz, 0.109		0.088 Hz, 0.094	
	$\lvert\varphi\rvert$	$\theta/(\pi\,\mathrm{rad})$	$\lvert\varphi\rvert$	$\theta/(\pi\,\mathrm{rad})$
P	1.000	0.000	1.000	0.000
P_w	6.177	−0.116	1.266	−0.061
Ω	0.006	−0.247	0.001	0.660
β	0.004	0.919	0.001	0.254
δ_x	0.011	−0.069	0.004	−0.678
δ_y	0.001	0.923	0.000	0.932
P_s	9.156	−0.037	1.899	0.503
$\Omega = \omega_e$	0.274	0.972	0.068	−0.410
P_h	14.246	0.926	1.672	−0.542
Ω	0.023	0.976	0.006	0.509
β	0.010	−0.452	0.001	0.233

modes have been normalized[11] such that the amplitude of the total electrical power – that absorbed by the electrical load – is equal to 1 MW, at zero phase angle.

The problematic behavior appears to be driven by the hydroelectric plant, whose frequency-droop control has been given a tuning that is too aggressive for use in this sort of isolated system, even though it was fine when the grid was strong (Fig. 28). The non-minimum phase behavior – that is, the fact that the initial response is opposite the command – causes the hydroelectric plant to oppose the steam and wind plants. This has consequences for the wind turbines' mechanical systems, as the oscillations in power are accompanied by blade pitch and tower motions.

Figure 31 shows what happens if the gain $K_{P\omega}$ (Table VII) is set to zero, such that the hydroelectric plant no longer provides frequency-droop control. It still responds to a change in load, via the influence of the voltage and frequency on the synchronous generator, but the plant's controls return the power to the original value. The thermal and wind plants provide the necessary power, through a favorable control dynamic, having a rapid rise time, with moderate overshoot and settling. It is possible to employ the hydroelectric plant for longer-term balancing, over several minutes, by setting the gate control low-pass filter to a suitably low frequency. Then the system experiences a dynamic where the thermal and wind plants provide an initial response, followed by a slow, settling response where the hydroelectric plant ramps up and the other plants down.

Finally, Fig. 32 shows the response of the system to a perturbation in the wind speed at one wind turbine. There is a strong component at the tower resonant frequency of 0.24 Hz. This signal is especially strong due to the use of the generator torque to actively damp tower side-to-side motions. The interaction is visible in the tower modes themselves, Table XII.

A tower signal was not seen in previous figures, where the input signal came via the dispatch controller. This is because a filter was applied to prevent the control signal from exciting the tower frequency.

On its own, normal atmospheric turbulence does not contain much energy in the frequency band above 0.1 Hz, nor would one expect the turbulent winds at turbines within the plant to be highly correlated. So what might excite the tower resonance? Well, 3P rotational sampling or a 1P rotor imbalance impart some energy at the tower frequency, as do ocean waves. On the plant scale, there could exist higher-order effects in the atmosphere or electrical system (not included in the present model) that over time might cause the rotors to synchronize. Were this the case, then Fig. 32 indicates that one would see a significant tower-frequency fluctuation appear in the generated power of the thermal plant, and to a lesser extent the hydropower plant. It could be advisable to install a filter at

---

[11]The magnitude and absolute phase of an eigenmode are arbitrary. Only the *relative* magnitudes and phases are meaningful, so one can always pick one variable as the reference, to be given a unit magnitude and zero phase.
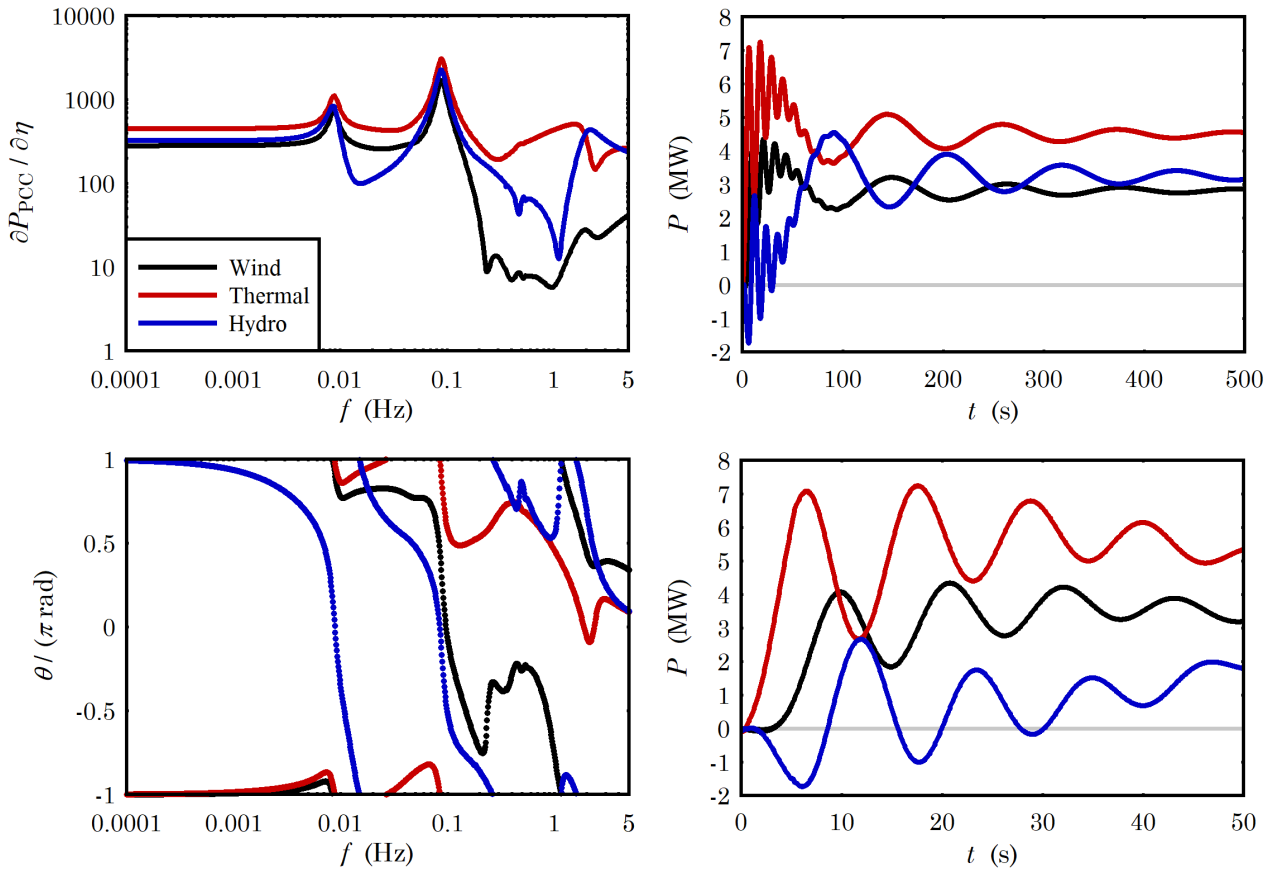
PROJECT
TotalControl

REPORT NUMBER
D4.6

VERSION
1.0

43 of 47

Figure 30: *The power-generation response to an increase in load (negative η). At left, the magnitude and phase of the transfer function. At right, the time response to a 5 s ramp from $\eta = 0$ to -0.01.*
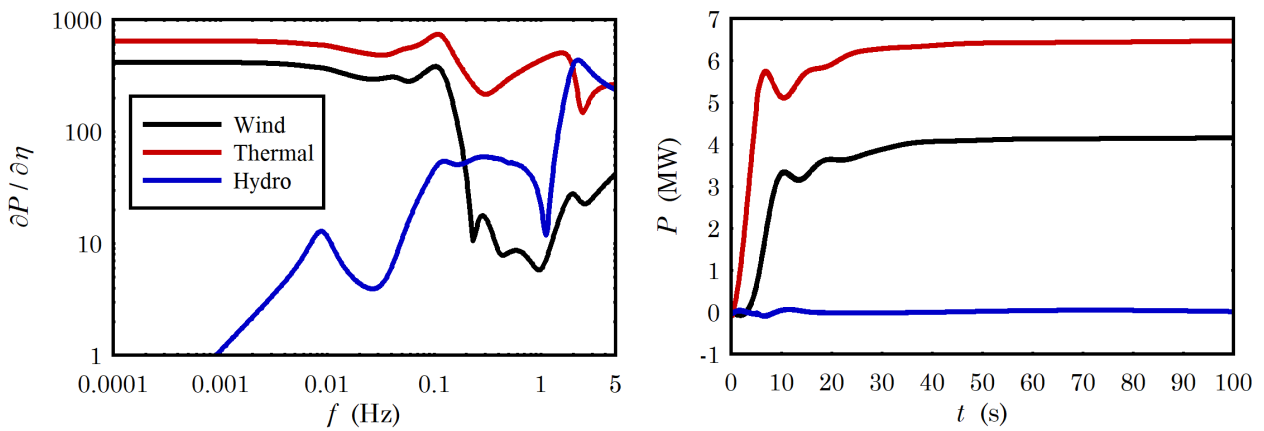

Figure 31: *The power-generation response without balancing from the hydroelectric plant, setting $K_{P\omega} = 0$ (Table VII).*

PROJECT
TotalControl

REPORT NUMBER
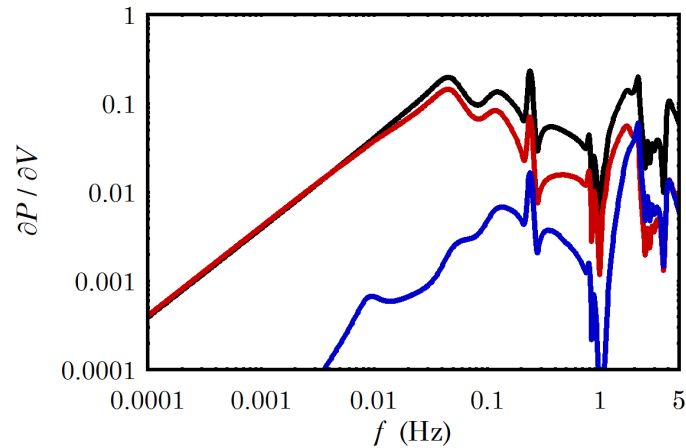D4.6

VERSION
1.0

44 of 47

Figure 32: The response of the system to a wind speed input at one turbine.

Table XII: Characteristics of the wind turbine tower resonant modes when grid-connected.

Variable	0.230 Hz, 0.062		0.239 Hz, 0.066	
	$\lvert\varphi\rvert$	$\theta/(\pi\,\mathrm{rad})$	$\lvert\varphi\rvert$	$\theta/(\pi\,\mathrm{rad})$
P_w	13.692	0.783	3.450	0.497
Ω	0.055	-0.681	0.032	0.983
β	0.036	0.147	0.014	-0.490
δ_x	1.230	0.912	1.000	0.000
δ_y	1.000	0.000	0.161	-0.013
P_s	3.686	-0.538	0.861	-0.817
$\Omega = \omega_e$	0.318	0.442	0.079	0.137
P_h	0.918	-0.001	0.235	-0.308
Ω	0.027	0.453	0.007	0.148
β	0.000	0.591	0.000	0.279

the *wind turbine*'s tower frequency in the power controller of interconnected power plants.

3.13   Recommendations and conclusions

The electrical and mechanical systems of a wind power plant are connected through the generator power controls. When the scope of the power control is expanded to include grid support functions, this links the dynamics of the wind turbine to the rest of the grid, potentially including other nearby power stations. The controls cannot be tuned in isolation and expected to work flawlessly when connected to the power grid. Rather, they should be tuned based on models such as that developed for the present work, containing a realistic representation of different generation sources and the broader electric grid.

   In particular, it was found that the effective impedance of the grid must be used for feedback linearization control of the wind turbines' network-side converters. If a hydroelectric plant is part of the generation mix, then its contribution to frequency support will likely be limited to slow timescales. This phenomenon is well known, however we saw how it becomes more severe once the plant is connected to other generating units on a weak grid; the controller should be tuned using the worst-case conditions expected on-site. Structural modes of the wind turbine feed through to the grid, especially when the generator is used for active damping, and may appear in the power control of other generating units. If this presents a problem, it should be straightforward to fix through appropriate filtering of the frequency droop controls, but this should be done based on a holistic model of the system dynamics.

PROJECT
TotalControl

REPORT NUMBER
D4.6

VERSION
1.0

45 of 47

References

Anaya-Lara O, *et al.* 2009. *Wind Energy Generation – Modelling and Control.* Wiley.

Anaya-Lara O, *et al.* 2018. *Offshore Wind Energy Technology.* Wiley.

Andersen, S., Madariaga, A., Merz, K., Meyers, J., Munters, W., and Rodriguez, C. 2018. Reference Wind Power Plant D1.03, TotalControl - Project no. 727680

Andersen, S. J., Meyers, J., Munters, W., Sood, I., and Troldborg, N.: Flow Database for reference wind farms part 1: precursor simulations, Tech. rep., DTU, KUL, `https://www.totalcontrolproject.eu/-/media/sites/totalcontrol/publications/public-deliverables/totalcontrol_d1_04_final.pdf?la=da&hash=B0047962A8135A4A8E75B01E3B0B8FE6D3DCD268`, 2019.

Andersen, S. J. and Troldborg, N. 2020. Description of TotalControl Reference Wind Farm Simulations, `https://doi.org/10.11583/DTU.13160606.v2`.

DNV, "International grid code listing," DNV, [Online]. Available: www.dnv.com/GridCodeListing.pdf. [Accessed 28 04 2022]

Eguinoa I, Göçmen T, Garcia-Rosa PB, *et al.* 2021. Wind farm flow control oriented to electricity markets and grid integration: initial perspective analysis. Advanced Control for Applications 2021; n/a(n/a): e80. e80 ADC2-21-0023; `https://doi.org/10.1002/adc2.80`

Endegnanew AG, et al. (2013). Design procedure for inter-array electric design. Report D2.2, EERA DTOC.

ENTSO-E. Requirements for Generators, "Entso-e," 16 April 2016. [Online]. Available: `https://www.entsoe.eu/network_codes/rfg/`.

FarmConners, "D2.1 A Position paper on certification, standardisation, and other regulatory issues of Wind Farm Control". Available at: `https://www.windfarmcontrol.info/publications`

Göçmen, T., Kölle, K., Andersen, S. J., Eguinoa, *et al.*: Launch of the FarmConners Wind Farm Control benchmark for code comparison, Journal of Physics:Conference Series, 1618, 022 040, `https://doi.org/10.1088/1742-6596/1618/2/022040`, 2020.

Göçmen,T., Campagnolo, F.,Duc, T., *et al.* "FarmConners Wind Farm Flow Control Benchmark: Blind Test Results" Wind Energy Science, `https://doi.org/10.5194/wes-2022-5`

Hille, N., Gehlhaar, T., *et al.* 2020 TotalControl, "D4.7 Design guidelines and standards"

Kundur P (1994). *Power System Stability and Control.* McGraw-Hill.

Merz KO (2018). *STAS Aeroelastic 1.0 – Theory Manual.* Report 2018:00834, SINTEF Energy Research.

Merz KO (2019a). STAS Actuator 1.0 – Theory Manual. Memo AN 19.12.06, SINTEF Energy Research.

Merz KO (2019b). STAS Electric 1.0 – Theory Manual. Memo AN 19.12.07, SINTEF Energy Research.

Merz KO (2019c). State-space model of a hydroelectric plant with Francis turbines. Memo AN 19.12.58, SINTEF Energy Research.

Merz KO (2020). *Development of an LQR framework for rapid prototyping of offshore wind turbine controllers, with application to active load control.* Report 2020:00257, SINTEF Energy Research.

Merz KO, Pedersen MD (2018). Offshore wind turbine controls. Chapter 5 of Anaya-Lara O, *et al.* (2018). *Offshore Wind Energy Technology.* Wiley.

Merz KO, *et al.* (2019). *An electromechanical model of the TotalControl Reference Wind Power Plant.* Report 2019:00342, SINTEF Energy Research.

Munters W and Meyers J (2018). Towards practical dynamic induction control of wind farms: analysis of optimally controlled wind-farm boundary layers and sinusoidal induction control of first-row turbines. Wind Energy Science 3: 409-425.

National Grid ESO (2019), Connection and Use of System Code, 1 April 2019. [Online]. Available: `https://www.nationalgrideso.com/codes/connection-and-use-system-code-cusc?code-documents`.

National Grid ESO (2019), The Grid Code, 4 September 2019. [Online]. Available: https://www.nationalgrideso.com/codes/grid-code?code-documents .

National Grid ESO (2022), "Reactive Reform – Market Design" [Online]. Available: `https://www.nationalgrideso.com/balancing-services/reactive-power-services/reactive-reform-market-design`

TotalControl, "D2.3 Optimization of WPP set-points" Available at `https://www.totalcontrolproject.eu/dissemination-activities/public-deliverables`

TotalControl, "D4.2 Hierarchic wind power plant supervisory controller" Available at `https://www.totalcontrolproject.eu/dissemination-activities/public-deliverables`

Acknowledgements

PROJECT
TotalControl

REPORT NUMBER
D4.6

VERSION
1.0

47 of 47